

AD-A164 126

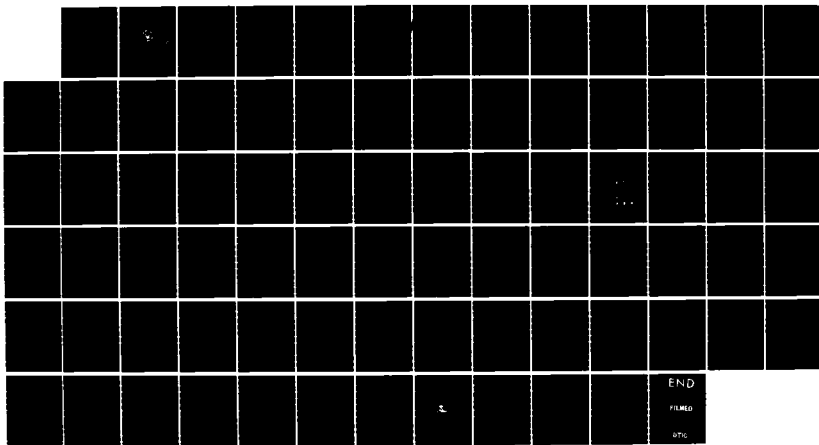
MEASUREMENT OF THE ACOUSTIC PRESSURE EVERYWHERE OVER A
MODELED CONTINENTAL SLOPE(U) NAVAL POSTGRADUATE SCHOOL
MONTEREY CA J A BORCHARDT DEC 85

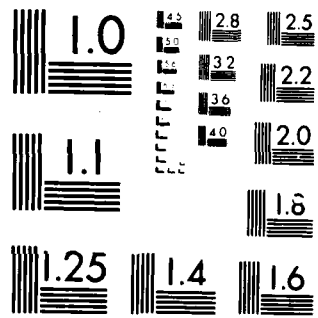
1/1

UNCLASSIFIED

F/G 20/1

NL





MICROCOPY RESOLUTION TEST CHART
NATIONAL BUREAU OF STANDARDS-1963-A

AD-A164 126

2

NAVAL POSTGRADUATE SCHOOL Monterey, California



DTIC
ELECTE
FEB 14 1986
S B

THESIS

MEASUREMENT OF THE ACOUSTIC PRESSURE
EVERYWHERE OVER A MODELED
CONTINENTAL SLOPE

by

John A. Borchardt

December 1985

Thesis Advisor:

J.V. Sanders

DTIC FILE COPY

Approved for public release; distribution is unlimited

86 2 14 076

UNCLASSIFIED

SECURITY CLASSIFICATION OF THIS PAGE

ADA 169126

REPORT DOCUMENTATION PAGE

1a REPORT SECURITY CLASSIFICATION			1b. RESTRICTIVE MARKINGS			
2a SECURITY CLASSIFICATION AUTHORITY			3 DISTRIBUTION/AVAILABILITY OF REPORT			
2b DECLASSIFICATION/DOWNGRADING SCHEDULE			Approved for public release; distribution is unlimited			
4 PERFORMING ORGANIZATION REPORT NUMBER(S)			5 MONITORING ORGANIZATION REPORT NUMBER(S)			
6a. NAME OF PERFORMING ORGANIZATION		6b OFFICE SYMBOL (if applicable)		7a. NAME OF MONITORING ORGANIZATION		
Naval Postgraduate School		Code 61		Naval Postgraduate School		
6c. ADDRESS (City, State, and ZIP Code)			7b. ADDRESS (City, State, and ZIP Code)			
Monterey, California 93943-5100			Monterey, California 93943-5100			
8a NAME OF FUNDING/SPONSORING ORGANIZATION		8b OFFICE SYMBOL (if applicable)		9. PROCUREMENT INSTRUMENT IDENTIFICATION NUMBER		
8c ADDRESS (City, State, and ZIP Code)				10 SOURCE OF FUNDING NUMBERS		
				PROGRAM ELEMENT NO.	PROJECT NO.	TASK NO.
						WORK UNIT ACCESSION NO.
11 TITLE (Include Security Classification)						
MEASUREMENT OF THE ACOUSTIC PRESSURE EVERYWHERE OVER A MODELED CONTINENTAL SLOPE						
12 PERSONAL AUTHOR(S)						
Borchardt, John A.						
13a TYPE OF REPORT		13b TIME COVERED		14 DATE OF REPORT (Year, Month, Day)		15 PAGE COUNT
Master's Thesis		FROM _____ TO _____		1985, December		79
16 SUPPLEMENTARY NOTATION						
17 COSATI CODES			18 SUBJECT TERMS (Continue on reverse if necessary and identify by block number)			
FIELD	GROUP	SUB-GROUP	Sound Pressure Field; Wedge-shaped Fluid; Substrate of Greater Sound Speed			
19 ABSTRACT (Continue on reverse if necessary and identify by block number)						
<p>An image model was used to predict the sound pressure field everywhere within isospeed water overlying a sloping absorbing bottom. All lengths scale with the dump distance, which is the distance from the apex of the wedge to the point where the depth is equal to the minimum uniform depth that can support propagation of the lowest normal mode. Measurements made in a laboratory tank with a 9.5° sand bottom with density and speed</p>						
20 DISTRIBUTION AVAILABILITY OF ABSTRACT				21 ABSTRACT SECURITY CLASSIFICATION		
<input checked="" type="checkbox"/> UNCLASSIFIED/UNLIMITED <input type="checkbox"/> SAME AS OTT <input type="checkbox"/> DTIC USERS				Unclassified		
22a NAME OF RESPONSIBLE INDIVIDUAL			22b TELEPHONE (include Area Code)		22c OFFICE SYMBOL	
Prof. J.V. Sanders			(408) 646-2931		Code 61Sd	

UNCLASSIFIED

SECURITY CLASSIFICATION OF THIS PAGE (When Data Entered)

#19 - ABSTRACT - (CONTINUED)

of sound 2.0 and 1.1 times those of water showed qualitative agreement with the predictions of the model for receiver distances up to 10 dump distances from the apex and 50 dump distances along the shore. *View is*

UNCLASSIFIED

SECURITY CLASSIFICATION OF THIS PAGE (When Data Entered)

Approved for public release; distribution is unlimited.

Measurement of the Acoustic Pressure
Everywhere Over a Modeled
Continental Slope

by

John A. Borchardt
Lieutenant Commander, United States Navy
B.S., United States Naval Academy, 1974

Submitted in partial fulfillment of the
requirements for the degree of

MASTER OF SCIENCE IN ENGINEERING SCIENCE

from the

NAVAL POSTGRADUATE SCHOOL
December 1985

Author:


John A. Borchardt

Approved by:


James V. Sanders, Thesis Advisor


Alan B. Coppens, Second Reader


Gordon E. Schacher, Chairman,
Department of Physics


John N. Dyer,
Dean of Science and Engineering

ABSTRACT

An image model was used to predict the sound pressure field everywhere within isospeed water overlying a sloping absorbing bottom. All lengths scale with the dump distance, which is the distance from the apex of the wedge to the point where the depth is equal to the minimum uniform depth that can support propagation of the lowest normal mode. Measurements made in a laboratory tank with a 9.5° sand bottom with density and speed of sound 2.0 and 1.1 times those of water showed qualitative agreement with the predictions of the model for receiver distances up to 10 dump distances from the apex and 50 dump distances along the shore.

TABLE OF CONTENTS

I.	INTRODUCTION -----	10
II.	PROGRAM DEVELOPMENT -----	16
III.	EXPERIMENTAL DESIGN AND PROCEDURES -----	18
	A. THE TANK -----	18
	B. SIGNAL GENERATING AND RECEIVING EQUIPMENT ----	20
	C. REFLECTION COEFFICIENTS -----	22
	D. EXPERIMENTAL CONSTANTS -----	23
	E. MEASUREMENT PROCEDURES AND CONSTRAINTS -----	24
IV.	RESULTS -----	26
	A. DEPENDENCE OF PRESSURE ON DEPTH FOR FIXED RECEIVER POSITION -----	26
	B. DEPENDENCE OF PRESSURE ON DISTANCE PARALLEL TO SHORE FOR FIXED RECEIVER DEPTH -----	29
	C. LOCI OF MAXIMUM PRESSURE -----	30
V.	CONCLUSIONS AND RECOMMENDATIONS -----	31
	APPENDIX: FIGURES -----	33
	LIST OF REFERENCES -----	76
	INITIAL DISTRIBUTION LIST -----	78



Accession For	
NTIS GRA&I	<input checked="" type="checkbox"/>
DTIC TAB	<input type="checkbox"/>
Unannounced	<input type="checkbox"/>
Justification	
By _____	
Distribution/	
Availability Codes	
Dist	Avail and/or Special
A-1	

LIST OF FIGURES

Figure	Title	Page
1.	Three-Dimensional Wedge Geometry -----	33
2.	Tank Configuration -----	34
3.	Electronic Equipment Configuration -----	35
4.	Type F-41 Transducer Directivity Patterns ---	36
5.	Type F-41 Transducer Electrical Characteristics -----	37
6.	LC-5 Hydrophone Characteristics -----	38
7.	Bottom Reflection Coefficients -----	39
8.	Sound Pressure in the Wedge, $Y_0=0$, $R_1=30$, $R_2=3$ -----	40
9.	Sound Pressure in the Wedge, $Y_0=0$, $R_1=30$, $R_2=5$ -----	41
10.	Sound Pressure in the Wedge, $Y_0=0$, $R_1=30$, $R_2=7$ -----	42
11.	Sound Pressure in the Wedge, $Y_0=0$, $R_1=30$, $R_2=9$ -----	43
12.	Sound Pressure in the Wedge, $Y_0=0$, $R_1=30$, $R_2=11$ -----	44
13.	Sound Pressure in the Wedge, $Y_0=10$, $R_1=30$, $R_2=3$ -----	45
14.	Sound Pressure in the Wedge, $Y_0=10$, $R_1=30$, $R_2=5$ -----	46
15.	Sound Pressure in the Wedge, $Y_0=10$, $R_1=30$, $R_2=7$ -----	47
16.	Sound Pressure in the Wedge, $Y_0=10$, $R_1=30$, $R_2=9$ -----	48
17.	Sound Pressure in the Wedge, $Y_0=10$, $R_1=30$, $R_2=11$ -----	49

18.	Sound Pressure in the Wedge, $Y_0=10$, $R_1=30$, $R_2=15$ -----	50
19.	Sound Pressure in the Wedge, $Y_0=10$, $R_1=30$, $R_2=20$ -----	51
20.	Sound Pressure in the Wedge, $Y_0=20$, $R_1=30$, $R_2=3$ -----	52
21.	Sound Pressure in the Wedge, $Y_0=20$, $R_1=30$, $R_2=5$ -----	53
22.	Sound Pressure in the Wedge, $Y_0=20$, $R_1=30$, $R_2=7$ -----	54
23.	Sound Pressure in the Wedge, $Y_0=20$, $R_1=30$, $R_2=9$ -----	55
24.	Sound Pressure in the Wedge, $Y_0=20$, $R_1=30$, $R_2=11$ -----	56
25.	Sound Pressure in the Wedge, $Y_0=30$, $R_1=30$, $R_2=3$ -----	57
26.	Sound Pressure in the Wedge, $Y_0=30$, $R_1=30$, $R_2=5$ -----	58
27.	Sound Pressure in the Wedge, $Y_0=30$, $R_1=30$, $R_2=7$ -----	59
28.	Sound Pressure in the Wedge, $Y_0=30$, $R_1=30$, $R_2=9$ -----	60
29.	Sound Pressure in the Wedge, $Y_0=30$, $R_1=30$, $R_2=11$ -----	61
30.	Sound Pressure in the Wedge, $Y_0=50$, $R_1=30$, $R_2=3$ -----	62
31.	Sound Pressure in the Wedge, $Y_0=50$, $R_1=30$, $R_2=5$ -----	63
32.	Sound Pressure in the Wedge, $Y_0=10$, $R_1=25$, $R_2=25$ -----	64
33.	Sound Pressure in the Wedge, $Y_0=20$, $R_1=25$, $R_2=25$ -----	65
34.	Sound Pressure in the Wedge, $Y_0=30$, $R_1=25$, $R_2=25$ -----	66

35.	Sound Pressure in the Wedge, $R_1=30$, $R_2=3$, D=4.75 -----	67
36.	Grid for Determining Sound Pressure in the Wedge -----	68
37.	Sound Pressure in the Wedge, $R_1=30$, $R_2=25$, D=4.75 -----	69
38.	Sound Pressure in the Wedge, $R_1=30$, $R_2=3.5$, D=4.75 -----	70
39.	Loci of Pressure Maxima in the Wedge, $Y_0=8$, D=4.75 -----	71
40.	Loci of Pressure Maxima in the Wedge, $Y_0=16$, D=4.75 -----	72
41.	Loci of Pressure Maxima in the Wedge, $Y_0=24$, D=4.75 -----	73
42.	Loci of Pressure Maxima in the Wedge, $Y_0=32$, D=4.75 -----	74
43.	Pressure in the Wedge as Calculated by Image Model, B=10, G=5, D=5, $R_1=40$ -----	75

ACKNOWLEDGEMENT

The author expresses his appreciation to Professors James V. Sanders and Alan B. Coppens for their support, advice and direction in this project. Also, I would like to thank Debra Lynn Borchardt for her support and understanding for the many lonely hours.

I. INTRODUCTION

A number of acoustic models have been developed to predict the sound pressure within a wedge-shaped fluid medium overlying a fluid bottom of greater sound speed. Each of these models contains inherent strengths and weaknesses as observed during experimental and theoretical analysis. The major problem with most of these models is the difficulty in applying boundary conditions at the bottom where there is an interface between two media of different densities and sound speeds.

The optical field in a wedge-shaped medium overlying a substrate with greater refractive index was investigated in 1971 by Tien and Martin [Ref. 1]. They examined the behavior of a laser beam coupled into a thin, tapered, transparent film deposited in a substrate with a greater refractive index. The results of this experiment showed that light propagating toward the apex was perfectly reflected until the grazing angle of incidence increased above the critical angle, then the light penetrated into the substrate.

In 1973, Kuznetsov [Ref. 2] studied an acoustical analog of Tien and Martin's optical problem. He developed a theory for sound propagation in both the wedge and the underlying medium that was based on adiabatic normal mode theory and a ray representation of normal modes. Kuznetsov concluded that:

1. Sound traveling toward the apex is totally reflected until the grazing angle of incidence increased above the critical angle.
2. At grazing angles of incidence greater than the critical some sound is refracted into the underlying half-space at each reflection until all the sound is transferred into the underlying half-space.
3. Acoustic energy in the half-space is collimated into a well-defined beam with the maximum pressure occurring at an angle of depression that lies between the wedge angle and twice the wedge angle.

Kuznetsov performed various experiments that verified his theory.

Lee and Papadakis [Ref. 3], in 1979, developed a technique for solving the parabolic equation that utilized an implicit finite-difference (IFD) algorithm. Their method incorporates appropriate boundary conditions, i.e., continuity of pressure and continuity of the normal component of particle velocity at an interface between media, and is useful for shallow water predictions. Jaeger [Ref. 4] developed the IFD algorithm into a computer model to predict transmission loss and acoustic pressure based on user-specified bottom topography and a single sound-speed profile. Jaeger's IFD procedure was tested by Kosnik [Ref. 5] in a laboratory shallow water environment. He concluded that no major flaws exist in the IFD model.

In 1978, Coppens, Sanders, Ioannou and Kawamura [Ref. 6] used image theory to predict the sound pressure along the bottom in the upslope direction. This model allowed varying

source depth and was available in two versions; one for a source at infinite distance and one for a source at finite distance.

In 1980, N. Bradshaw [Ref. 7] extended the computer model first developed by Kawamura and Ioannou to describe the sound pressure field in the bottom. Her predictions agreed qualitatively with the earlier work of Netzorg [Ref. 8] who made measurements in brine separated from a fresh water wedge by a thin mylar membrane. However, Netzorg's work did not meet all of Bradshaw's model constraints. J. Bradshaw [Ref. 9] studied the possibility of using a sand bottom for the experiment. He determined that a deaerated sand-water mixture behaved as a fluid for normal and oblique reflection of sound.

In January, 1984, Coppens, Humphries and Sanders [Ref. 10] extended the method of images by employing Green's Theory to predict the propagation of sound out of the wedge into the bottom. In this analysis, saddle-point approximations were used with both lossy and lossless substrate cases. While the saddle-point approximation is limited to a region directly under the apex of the wedge, it does allow prediction of the sound field in the substrate for any values of absorption in the substrate. They concluded that the method of images approach provides intrinsically the phase-interference effects associated with multiplicity of beams

entering the substrate. In addition, they concluded that the image approach appears to avoid the generation of caustics at the turning points which are obtained during the use of unmodified ray tracing approaches.

In 1984, Baek [Ref. 11] developed a model to predict the sound pressure amplitude and phase within the wedge in the upslope direction. Baek developed a computer program, titled WEDGE, that utilized a source at infinity. Baek's program was verified for several simple cases, such as a pressure release bottom and a rigid bottom.

Using data obtained by Kosnik [Ref. 5] LeSesne [Ref. 12] verified the accuracy of the predictions of WEDGE for the pressure field in the directly upslope direction.

Until recently, there has been no quantitative study of the sound field other than in the upslope direction. This situation was rectified when Coppens [Ref. 13] developed a computer model, named CROSS SLOPE, to predict the sound pressure field everywhere within the wedge-shaped fluid medium.

Computer predictions based on CROSS SLOPE were obtained by LeSesne [Ref. 13] and compared to the IFD model predictions and to experimental results obtained by Kosnik [Ref. 5].

LeSesne concluded that

1. The CROSS SLOPE program has a much shorter execution time and is more versatile than the IFD model, which is restricted to upslope and downslope propagation only,
2. The predictions of CROSS SLOPE are not inconsistent with the normal mode theory of Buckingham [Ref. 14].

Further, LeSesne recommended that an experiment be conducted to measure the pressure field across the slope. The purpose of this research was to

1. obtain detailed measurements of the sound pressure field in a wedge-shaped fluid medium over a bottom of greater sound speed,
2. compare measured amplitudes with those predicted by CROSS SLOPE and evaluate any observed inconsistencies,
3. provide output in a graphic form for ease of comparison,
4. recommend further course of action for related follow-on work.

All distances measured in the tank are normalized in terms of a basic unit called the dump distance. A dump distance x is defined as the distance measured perpendicular to the shore from the apex to the point where the depth is equal to the minimum uniform depth that can support propagation of the lowest normal mode. Specifically [Ref. 9]

$$x \equiv \lambda / (4 * \sin \theta_c * \tan \beta)$$

where λ is the wavelength of the sound in the medium, θ_c is the grazing critical angle at the bottom ($\theta_c \equiv \cos^{-1}(c_1/c_2)$), and c_1 and c_2 are the speeds of sound in the wedge and bottom respectively.

The following definitions will be used throughout:

- β = wedge angle
- R_1 = distance of the source from the shore normalized to the dump distance

- R_2 = distance of the receiver from the shore normalized to the dump distance
- Y_0 = distance along the shore between the source and receiver normalized to the dump distance
- D = receiver angle measured upward from the bottom
- G = source angle measured upward from the bottom
- D_1 = ratio of the water density to the bottom density (density ratio)
- cc = ratio of the speed of sound in the water to the speed of sound in the bottom (speed of sound ratio)
- XL = wave number in the water divided into the absorption in the bottom

A typical geometry for the cross-slope condition is shown in Fig. 1.

II. PROGRAM DEVELOPMENT

As previously noted, CROSS SLOPE was developed by Coppens [Ref. 10] to predict the sound pressure field everywhere within a wedge-shaped fluid medium over an absorbing fluid bottom of greater sound speed. This initial program was initially developed on a Wang computer using Interpretive Basic and had a very long execution time.

Legesne [Ref. 12] converted CROSS SLOPE to Fortran and designed it for use on the IBM 3033 computer at the Naval Postgraduate School. In this modified program several sub-routines and function calls were utilized to reduce the execution time. Several other options to reduce execution time were investigated by Legesne. The use of compilers, which could reduce execution time by a factor of ten, was examined. This method of computation was rejected because the program modifications that would have been needed would have made the program more hardware dependent. A second method examined was the use of a math co-processor in the IBM personal computer. This method was also rejected because compiler usage was required thus increasing hardware dependence. The final alternative examined was to program in Fortran using double precision arithmetic and utilize the IBM 3033 computer. The overriding factor for choosing this method was the increased speed of execution while

keeping the program relatively hardware independent. Comparisons between predictions of the original CROSS SLOPE and LeSesne's version showed agreement within 0.0003%. This acceptable error is caused by the difference in precision between the Wang and IBM 3033 computers.

Three different programs, based on CROSS SLOPE, were developed by LeSesne: SSLOPE, XSLOPE and XSLOPE1. These three programs are compatible and differ only in the format of their outputs. SSLOPE predicts pressure amplitude for fixed source position with receiver position and depth being the variables. XSLOPE predicts the pressure amplitude for a constant-depth receiver with source-receiver separation along the shoreline (Y_0) and receiver distance from the shoreline (R_2) being the variables. XSLOPE1 predicts the loci of the maximum pressure amplitude for constant receiver depth.

SSLOPE and XSLOPE predictions were used extensively in the experiment. XSLOPE1 predictions were verified to a lesser extent.

III. EXPERIMENTAL DESIGN AND PROCEDURES

A. THE TANK

A fiberglass encased wooden tank was used for the experiment. The tank dimensions were 304 cm (length), 117 cm (width) and 95 cm (depth). #30 fine sand filled most of the tank, leaving a 9.5° ($\pm 0.2^\circ$) wedge of water with the shoreline running the length of the tank. The maximum water depth in the tank was 20 cm. Measurements were made only in the middle 200 cm of the tank's length. The basic setup of the tank is shown in Fig. 2.

Fresh water and #30 fine sand were the media used in the experiment. The grain size for #30 fine sand varies from 0.15 mm to 0.70 mm. This grain size was considered small enough to not affect the experiment even at the highest frequency.

The shaping of the bottom to a uniform wedge angle proved to be a very long and tedious evolution. To form the wedge, a scraping device was designed and built to run on rollers placed on the long sides of the tank. After scraping out a wedge of approximately the correct shape, holes were drilled in the wooden blade to allow water trapped behind the blade during motion to escape easily, further smoothing the surface of the sand. After many passes with this configuration a thin rubber blade was added to the assembly

for the final smoothing operation. The entire evolution was constantly hampered by silt leaching out of the sand and becoming suspended in the water thus making it impossible to see the bottom. This problem was lessened by performing several flushes of the water. The flushes however did not completely remove the residue necessitating a wait of several hours after each set of passes by the scraper to allow the residue to settle.

The wedge angle was $9.5^\circ (\pm 0.2^\circ)$ and was kept constant throughout the experiment. At the end of each day's work, water was added to the tank to completely cover the sand thereby preventing any of the sand from drying out. At the beginning of each day's run the shoreline was reformed by removing a small amount of water from the tank to expose the sand near the apex. Thus, a small amount of water in the tank was replenished on a daily basis. The replenishment water was kept in a holding tank and allowed to sit for several days to permit air bubbles to escape prior to use. Air had been removed from the water-sand mixture upon installation by the use of a high-pressure water jet [Ref. 5]. Bleach was periodically added to the test and holding tanks to inhibit biological growth.

A slope of 9.5° was utilized to be consistent with previous experiments thereby allowing the facility to be tested by comparison with the results measured directly

upslope by Kosnik [Ref. 5]. A large slope was chosen to minimize the size of the dump distance thereby maximizing the number of dump distances that the source could be moved away from the apex allowing a better simulation of a distant source. While this slope is greater than encountered in most ocean environments, it is small enough to be considered realistic.

B. SIGNAL GENERATING AND RECEIVING EQUIPMENT

A schematic of the equipment is shown in Fig. 3. The 150 kHz output from a General Radio model 1310 oscillator was fed into a General Radio Type 396-A tone burst generator set to form a 16-cycle 4-V peak amplitude pulse. The output of the tone burst generator was passed through a Hewlett-Packard HP 467-A power amplifier set to X1 amplification before being fed to the transducer. The received signal was amplified 20 dB by a Hewlett-Packard HP-465A amplifier, then passed through a Spencer-Kennedy Laboratories, Inc. model 302 variable filter set to pass frequencies from 130 kHz to 170 kHz. The signal was then fed to a Nicolet Murel oscilloscope for analysis.

The acoustic source was the USRD Type F41 Transducer. This transducer consists of twelve 1.27-cm-diameter by .254-cm-thick lead zirconate-titrate elements cemented to high-density Kenna-metal disks. The array is approximately 3.8 cm wide and 5 cm high. The transducer face is circular with a diameter of 10 cm. Corprene is the pressure-release material around each of the elements, which are sealed in transparent polyurethane.

Castor oil is the acoustic coupling medium between the polyurethane potting compound and the butyl-rubber acoustic window. The directivity in the horizontal plane is broader than in the vertical plane because of the dimensions of the crystal array. The patterns are symmetrical and, at frequencies above 25 kHz, the back radiation is 19 to 22 dB below the front radiation. Typical directivity patterns in the horizontal and vertical planes are shown in Fig. 4. The specifications for the Type F41 transducer are:

Frequency range:	15 to 150 kHz
Transmitting voltage response (at 150 kHz):	160 dB re $ \mu\text{Pa} V$ at 150 kHz)
Maximum driving voltage:	200 Vrms
Nominal capacitance:	12000 pF
D-C resistance:	greater than 1000 Mohms
Maximum hydrostatic pressure:	3.4 MPa (340-m depth)
Operating temperature range:	0 to 35°C

Typical electrical characteristics are shown in Fig. 5.

The F41 transducer was chosen for the experiment primarily due to its high directivity and frequency range (150 kHz desirable for the experiment).

The acoustic receiver used for the experiment was the LC-5 omni-directional hydrophone consisting of a 1/16 inch diameter by 1/8 inch long barium titanate cylinder. Nominal specifications for the LC-5 hydrophone are

Frequency range:	1 to 600 kHz
Capacitance:	350 pF

D-C resistance:	greater than 1000 Mohm
Maximum static pressure:	50 psi
Voltage/pressure conversion:	-124 dB re 1V/ μ bar
Horizontal directivity ± 2 dB:	600 kHz
Operating temperature range:	-40 to +100 °C

The frequency response and typical directivity patterns for the LC-5 hydrophone are shown in Fig. 6. The LC-5 hydrophone was chosen for this experiment because of its small size and high sensitivity. The small size was necessary to make measurements close to the shoreline.

All equipment used in the experiment were on-shelf and readily available.

C. REFLECTION COEFFICIENTS

A speed of sound ratio of 0.90, a density ratio of 0.50, and an absorption coefficient of 0.10 had been previously determined by Kosnik [Ref. 5] and utilized by LeSesne [Ref. 12] in his model predictions. These values were also used for this experiment. In addition, pressure reflection coefficients were measured in the tank while the bottom was still level and compared with those predicted by

$$R = \frac{(r_2/r_1) - \psi}{(r_2/r_1) + \psi} \quad (1)$$

where ψ is

$$\psi = \sqrt{1 - (c_2/c_1 \sin \theta_i)^2} / \cos \theta_i \quad (2)$$

where θ_1 is the angle of incidence measured from the normal. The characteristic acoustic impedances of the water and sand (r_1 and r_2 respectively) were calculated by the following equation:

$$r = \rho C \quad (3)$$

The critical angle was calculated to be 66.8 degrees. Fig. 7 shows predicted and measured values of reflection coefficients at 150 kHz for varying angle of incidence (θ_1). These measurements were performed with a deep (50 cm) layer of water over the sand so that a single reflection pulse could be isolated for measurement. This figure shows excellent quantitative and qualitative agreement between predicted and observed values thus verifying that the correct density and speed of sound ratios were utilized and that good measurement procedures were being observed.

D. EXPERIMENTAL CONSTANTS

A frequency of 150 kHz was chosen since it is the highest frequency compatible with the available equipment and therefore minimized the dump distance. Minimizing the dump distance was necessary if the field at large dump distances was to be studied.

At 150 kHz, the dump distance (X) is 3.3 cm. Because of the different frequency utilized, this dump distance is smaller than the value used by LeSesne.

The wedge angle was $9.5^\circ (\pm 0.2^\circ)$ and was kept constant throughout the experiment.

E. MEASUREMENT PROCEDURES AND CONSTRAINTS

The sound pressure within the water was determined by positioning the receiver in the water at various depths and distances from the source.

Throughout the experiment the source angle measured from the bottom was held constant at 5.2° . This angle was used to ensure that the source was always clear of the bottom and the surface and that the axis of the acoustic field was approximately mid-way between the surface and bottom of the water.

The distance of the source from the shoreline (R_1) was varied between 25 and 30 dump distances. At a distance of less than 25 the source came too close to either the sand or the surface of the water. The maximum source distance of 30 dump distances was dictated by the width of the tank.

The distance of the receiver from the shoreline (R_2) was varied between 3 and 25 dump distances. At a distance of less than 3 dump distances the acoustic center of the LC-5 could not be placed in the water without the bottom of the LC-5 penetrating the sand beneath it.

Source and receiver separation parallel to the shoreline (Y_0) was varied between 0 and 50 dump distances; 50 dump distances being the limiting shoreline separation due to tank size constraints.

All position measurements were subject to both accuracy and precision errors. The error in reading the position of the receiver was ± 0.2 cm. The draining and refilling of the tank on a daily basis also created a positioning error since it was impossible to ensure that the same water level was utilized. Also, the bottom profile of the tank was not exactly uniform. This was due to the problems encountered during the wedge formation process. The effect of these variations was to cause small variations in the local wedge angle thus affecting the dump distance calculation. It is estimated that the accuracy error was less than 0.3 dump distances in source and receiver positioning.

The ability to store the received pulses using the Nicolet oscilloscope aided in obtaining accurate estimates of the pulse amplitude and allowed the analysis of a considerable amount of data in the limited time frame.

IV. RESULTS

A. DEPENDENCE OF PRESSURE ON DEPTH FOR FIXED RECEIVER POSITION

To allow the measured pressure amplitude to be compared to the predictions of the various computer predictions, the observed pressures were normalized by dividing by the maximum pressure measured during each run.

The majority of the measurements taken during the experiment consisted of variable-depth receiver data for fixed source and receiver position. These data could be easily compared with SSLOPE predictions. The following values of Y_0 (normalized distance measured along the shoreline) were used for this portion of the experiment: 0, 10, 20, 30, 50. For each of these values of Y_0 the following values of R_2 (normalized distance from the apex to the receiver measured perpendicular to the shoreline) were used: 3, 5, 7, 9, 11, 15, 20.

Figs. 8 through 12 show the predicted and experimental normalized pressure amplitudes as a function of receiver depth for the upslope condition ($Y_0 = 0$). Good agreement between predicted and experimental results is observed with the receiver close to the shore. As the distance of the receiver from the shore increases one sees the progressively increasing complexity of the predicted and observed pressure fields and a deteriorating agreement between these fields. Fig. 8 shows excellent quantitative agreement between predicted and experimental data.

Figs. 9 and 10 show qualitative agreement between predictions and observations. It is evident from Figs. 11 and 12 that the experimental equipment did not reproduce the fine structure predicted. This discrepancy is consistent with the experimental constraints and limitations discussed in Chapter III. Indicated on Figs. 11 and 12 is the approximate transducer length converted to normalized receiver angle. The received signal is an "average" of the pressure over this distance. In all cases where the receiver was capable of resolving the structure of the field, the scale of the features observed was consistent with the predicted scales.

All data are presented, regardless of whether the receiver was physically capable of resolving the fine structure of the pressure field. The experimental and predicted data greater than 10 dump distances from the shore are presented to illustrate the progressively increasing complexity of the observed pressure field as the distance of the receiver from the apex is increased.

Figs. 13 through 19 depict normalized pressure amplitude observations and predictions for $Y_0 = 10$. Again, good agreement is observed for small values of R_2 (3,5) and the agreement diminishes as the distance of the receiver from the shore is increased. Fig. 15 ($R_2 = 7$) shows fair agreement between predicted and experimental results with a slight difference of approximately 0.15 units of normalized receiver angle between the two sets of data. Figs. 16 through 18 show large disagreement between predicted and experimental data. Although most

of the major predicted peaks were observed, the majority of the fine structure was not. These data are consistent with the experimental constraints and the inability to take data with sufficient spatial resolution. Comparison of Figs. 13 through 19 clearly shows the rapid change in complexity of the pressure field over a relatively small change in receiver distance from the shore (17 dump distances).

Figs. 20 through 24 display constant-position, variable-depth predictions and observations for $Y_0 = 20$. The same general trends as previously noted were observed. Fig. 23 shows fair qualitative agreement between observed and predicted pressure amplitude with a slight shift in normalized receiver angle between the two curves. This figure is a good example of the effects of an error in receiver positioning geometry on local wedge angle.

Figs. 25 through 29 compare observed pressure amplitudes to SSLOPE predictions for $Y_0 = 30$. This data follows the general, qualitative trends previously discussed.

The maximum source-receiver separation along the shoreline (Y_0) attainable was 50. Figs. 30 and 31 compare the predicted and observed normalized pressure amplitudes for receiver distances from the shoreline (R_2) of 3 and 5 respectively. Again, good agreement is observed. Qualitative comparison between observed data at the same value of R_2 but different Y_0 show that the field is less complex the larger the receiver-source separation is.

The following general observations can be made about the fixed-position, variable-depth source measurements:

1. The complexity of the pressure field increased as receiver distance from the apex (R_2) increased. This fact led to the inability to quantitatively compare observed and predicted values for an R_2 of greater than 9-11 dump distances.
2. Slight variations in source positioning geometry (Y_0 , R_2 , receiver angle) led to vastly different results.
3. The pressure amplitude field complexity decreased as the source-receiver separation along the shoreline (Y_0) was increased.

Figs. 32, 33 and 34 compare observed normalized pressure amplitudes with SSLOPE predictions for the directly across-slope condition. For this case $R_1 = R_2 = 25$ and Y_0 was varied in increments of 10. As shown from these figures, the predicted pressure amplitude field is complex as is the observed pressure amplitude field. Quantitative analysis was not possible.

During many of the previous data runs (SSLOPE comparisons) the orientation of the acoustic axis of the source was varied in the horizontal plane. As would be expected, the best agreement between predictions and observations was obtained when the source and its associated images were pointing as nearly as possible towards the field point.

B. DEPENDENCE OF PRESSURE ON DISTANCE PARALLEL TO THE SHORE FOR FIXED RECEIVER DEPTH

The sound pressure field was measured at constant depth, $R_1 = 30$, $R_2 = 3$ and varying Y_0 from 0 to 50. These observed pressure amplitudes are compared against XSLOPE predictions in Fig. 35. As is evident from this figure, experimental and

predicted results showed very little agreement. To evaluate whether the cause of this was an error in receiver position, a grid of computer predictions that encompassed the assumed receiver position was formulated. This grid is depicted in Fig. 36. In order to ensure that the actual receiver position was within this grid R_2 was varied from 2.5 to 3.5 and D (receiver angle) was varied from 3.75° to 5.50° . The results for these predictions compared against the experimental data are shown in Figs. 35, 37 and 38. Again, qualitative agreement was not observed within the grid. This disagreement is attributed to the experimental constraints previously discussed, receiver positioning error and local wedge angle variation across the slope. These figures do show how rapidly the sound pressure field changes in the wedge.

C. LOCI OF MAXIMUM PRESSURE

The final portion of the experiment concerned verification of the XSLOPE program predictions. XSLOPE predicts the location and amplitude of the maximums for a given R_1 . Figs. 39 through 42 show the predicted results compared to observed data for $Y_0 = 8, 16, 24$ and 32 respectively. Excellent agreement between predicted and experimental results was observed for the case where $Y_0 = 8$. It clearly showed the buildup of maximums to a final peak and then a sharp drop-off as predicted by LeSesne and shown in Fig. 43. As Y_0 was increased, the quantitative agreement between predicted and experimental results diminished, however, the qualitative agreement remained and the general forms of the curves were consistent.

V. CONCLUSIONS AND RECOMMENDATIONS

The following conclusions are possible.

This analysis of Coppen's acoustic model did not uncover any major failures of model performance close to the shoreline (less than approximately 10 dump distances) in a simplified shallow water environment. In general, qualitative agreement between predicted and experimental data was observed however, the fine structure of the more complex fields could not be observed due to experimental constraints.

The acoustic pressure field becomes increasingly complex as the distance from the apex is increased. Quantitative verification of the model at distances from the apex of greater than approximately 10 dump distances was not possible because at these distances the structure of the pressure field required more spatial resolution than possible with the available equipment.

Minor variations of receiver depth, receiver distance from the apex and local wedge angle have a pronounced effect on the observed sound pressure field. Precise sculpting of the bottom is essential for accurate results.

Further study of the CROSS SLOPE model is recommended. Area of study should be concentrated on the across-slope scenario at distances from the apex of greater than 10 dump distances. Further, it is recommended that the following equipment modifications be made:

- 1) Use of a physically smaller source to allow increased mobility within the wedge.
- 2) Use of a larger tank, several of which are currently available at the Naval Postgraduate School, to study the acoustic pressure field at large dump distances (greater than 50 dump distances). This poses a problem in that it will make the sloping operation more tedious and logistically difficult.
- 3) Although the LC-5 proved to be an excellent receiver for the experiment, use of a smaller receiver would allow measurements to be made closer (less than three dump distances) to the apex.

Continued use of the CROSS SLOPE programs on the 3033 computer for future predictions is highly recommended.

APPENDIX

FIGURES

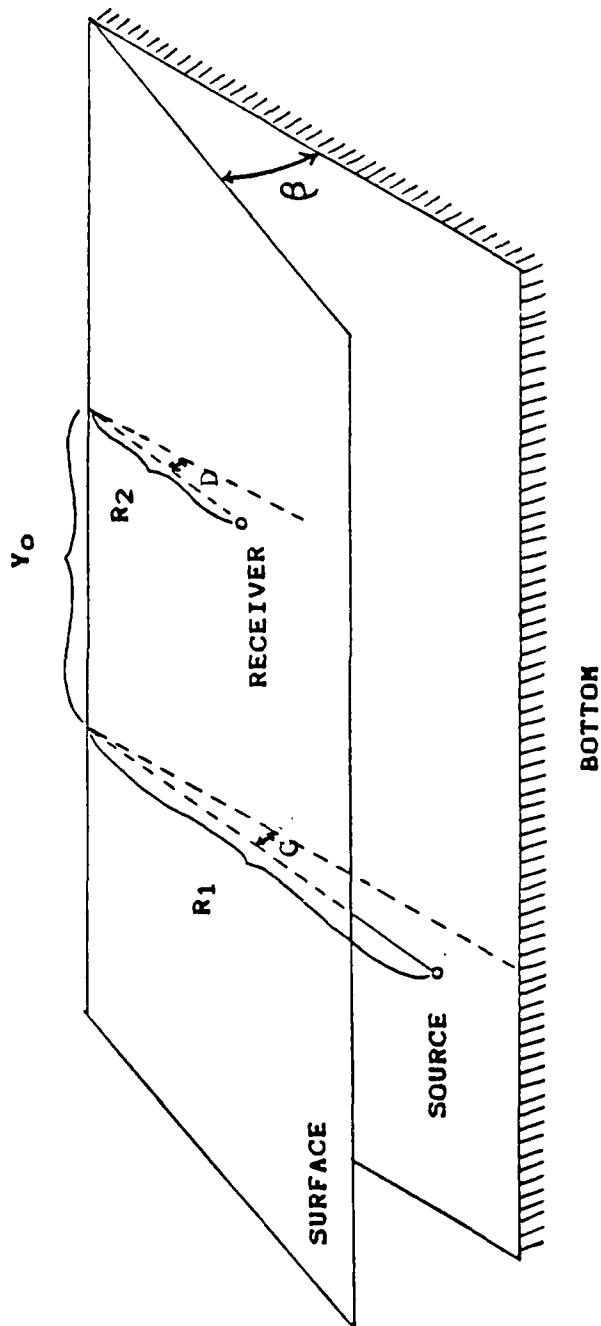


Figure 1. Three-Dimensional Wedge Geometry

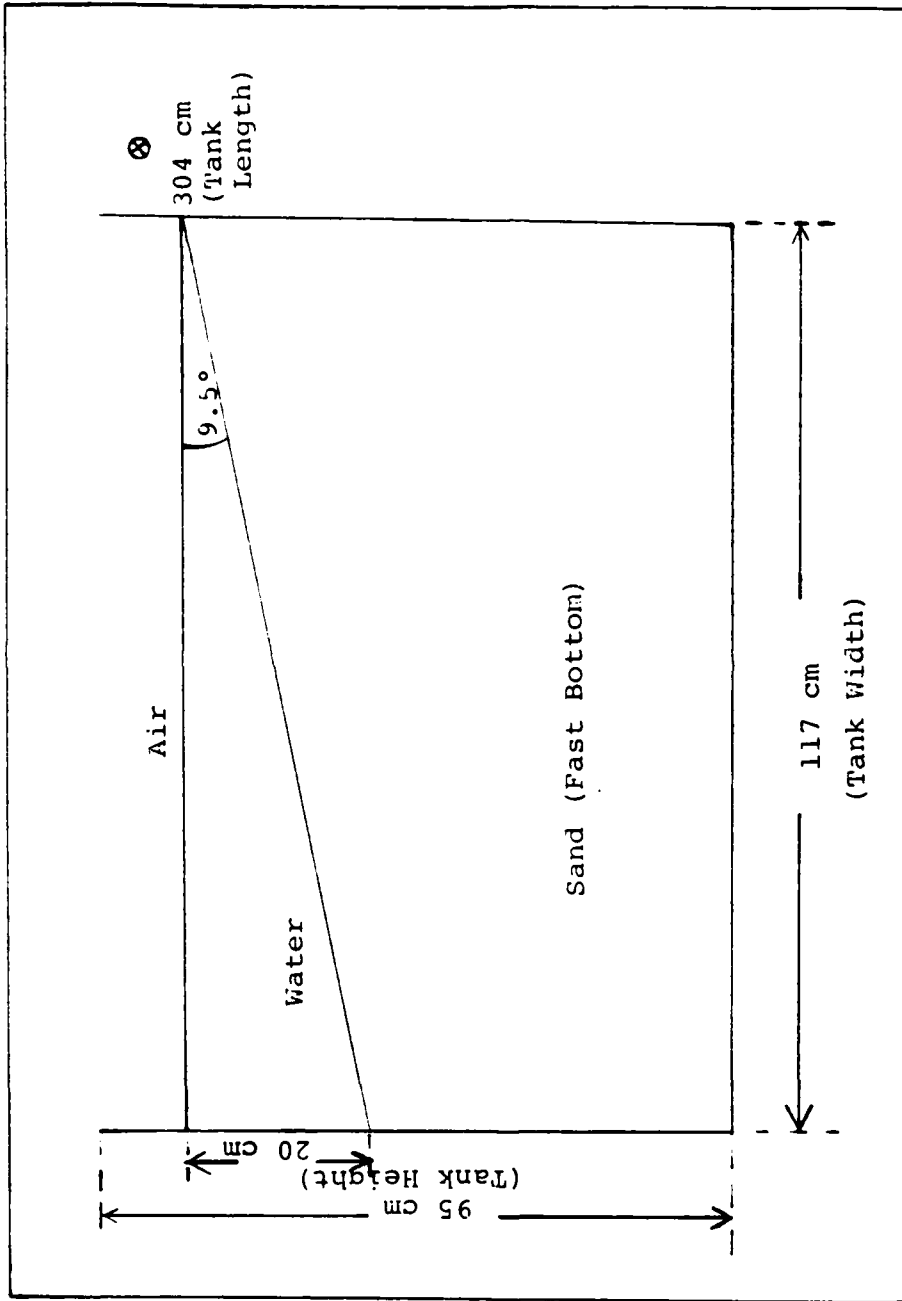


Figure 2. Experimental Tank Set UP

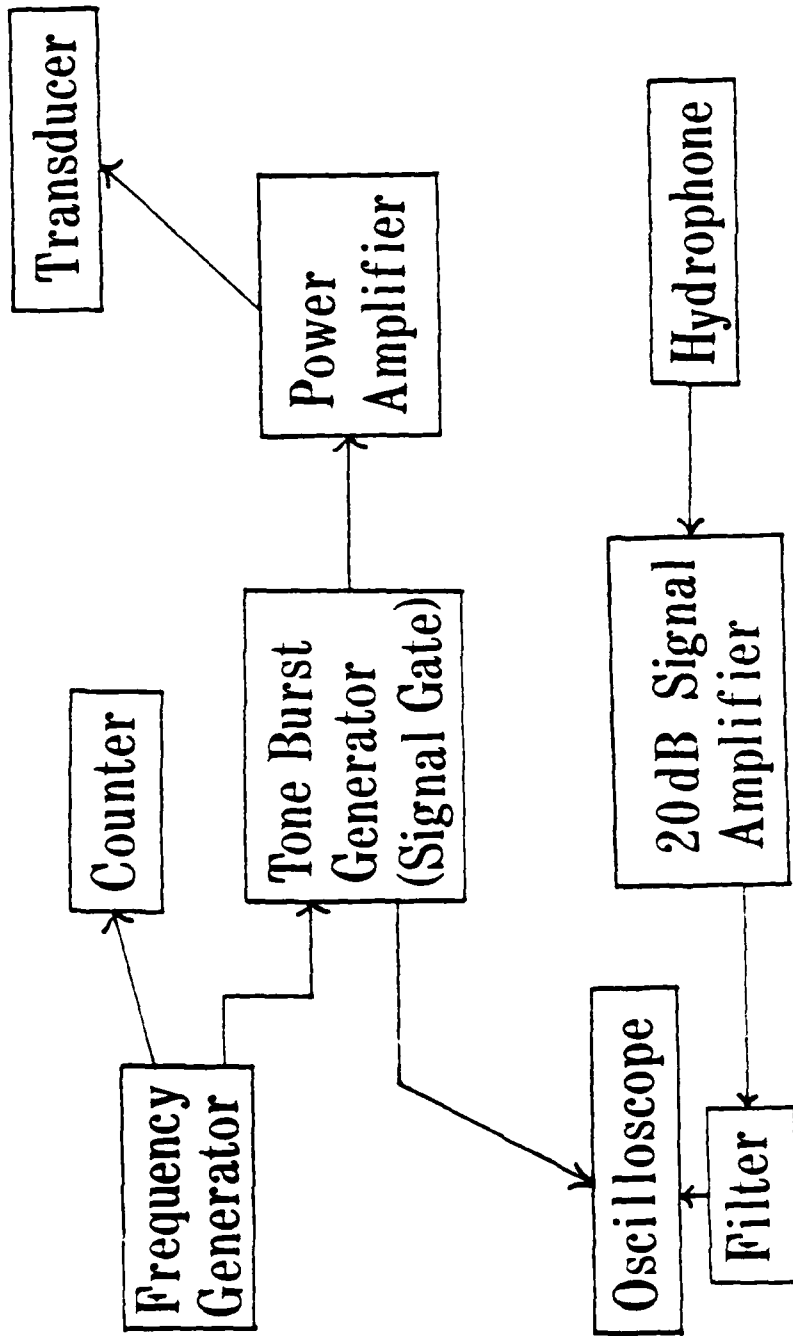
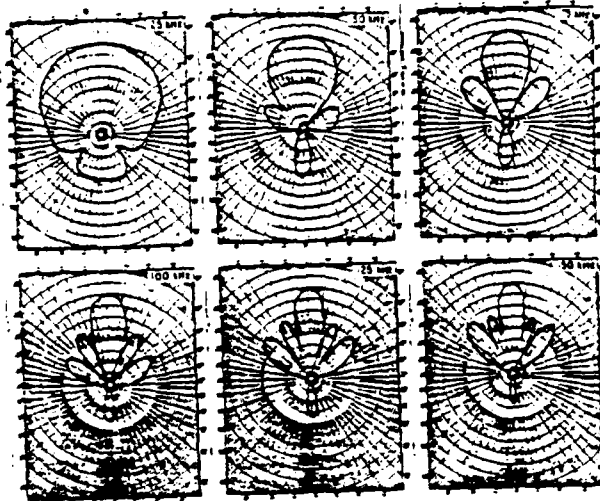


Figure 3. Electronic Equipment Schematic

a. Typical directivity patterns in the XY (horizontal) plane, type F41 transducer. Scale: center to top of grid, each pattern, equals 50 dB.



b. Typical directivity patterns in the XZ (vertical) plane, type F41 transducer. Scale: center to top of grid, each pattern, equals 50 dB.

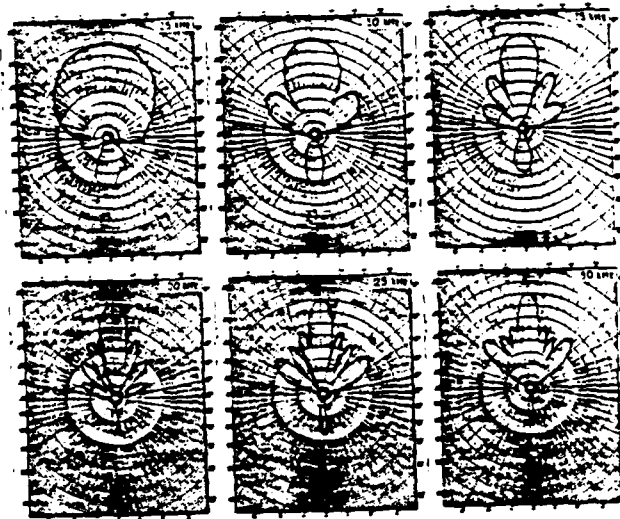
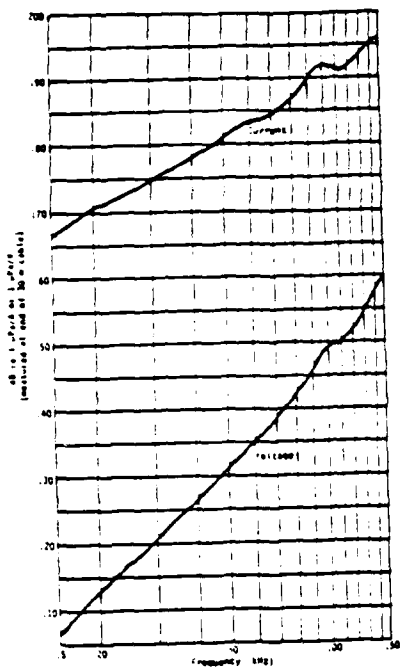
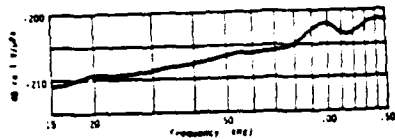


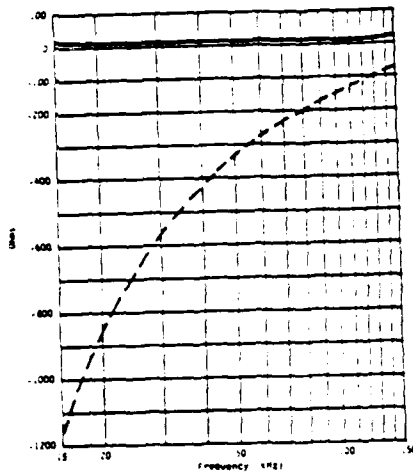
Figure 4. Type F-41 Transducer Directivity Patterns



a. Typical transmitting current and voltage responses, type F41 transducer.

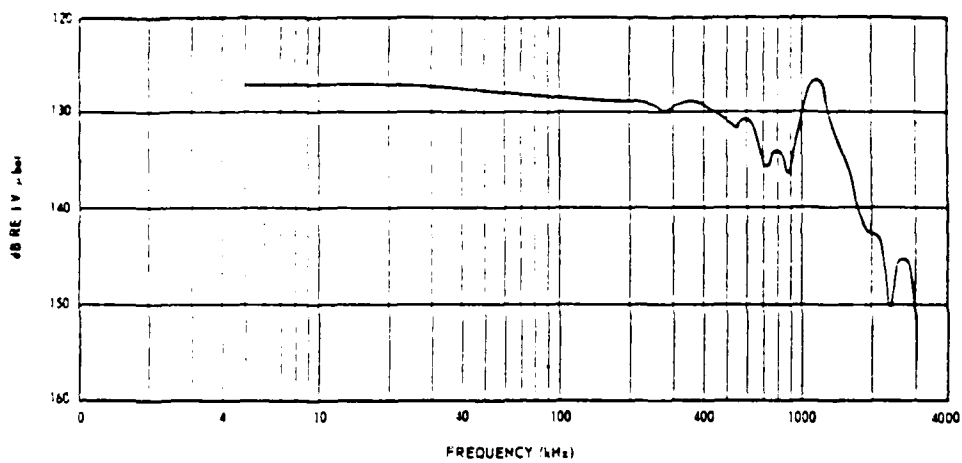


b. Typical free-field voltage sensitivity, type F41 transducer.

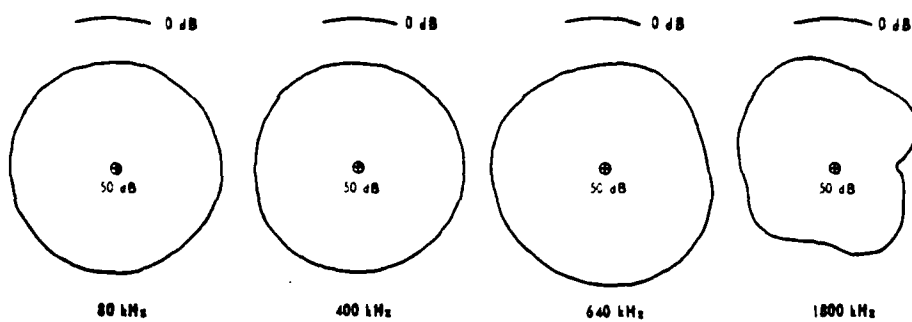


c. Typical Equivalent series impedance, type F41 transducer.

Figure 5. Type F-41 Transducer Electrical Characteristics



Typical free-field voltage sensitivity, the LC-5 hydrophone open-circuit voltage at end of 4-foot low noise cable.



Typical directivity patterns in the XY plane

Figure 6. LC-5 Hydrophone Characteristics

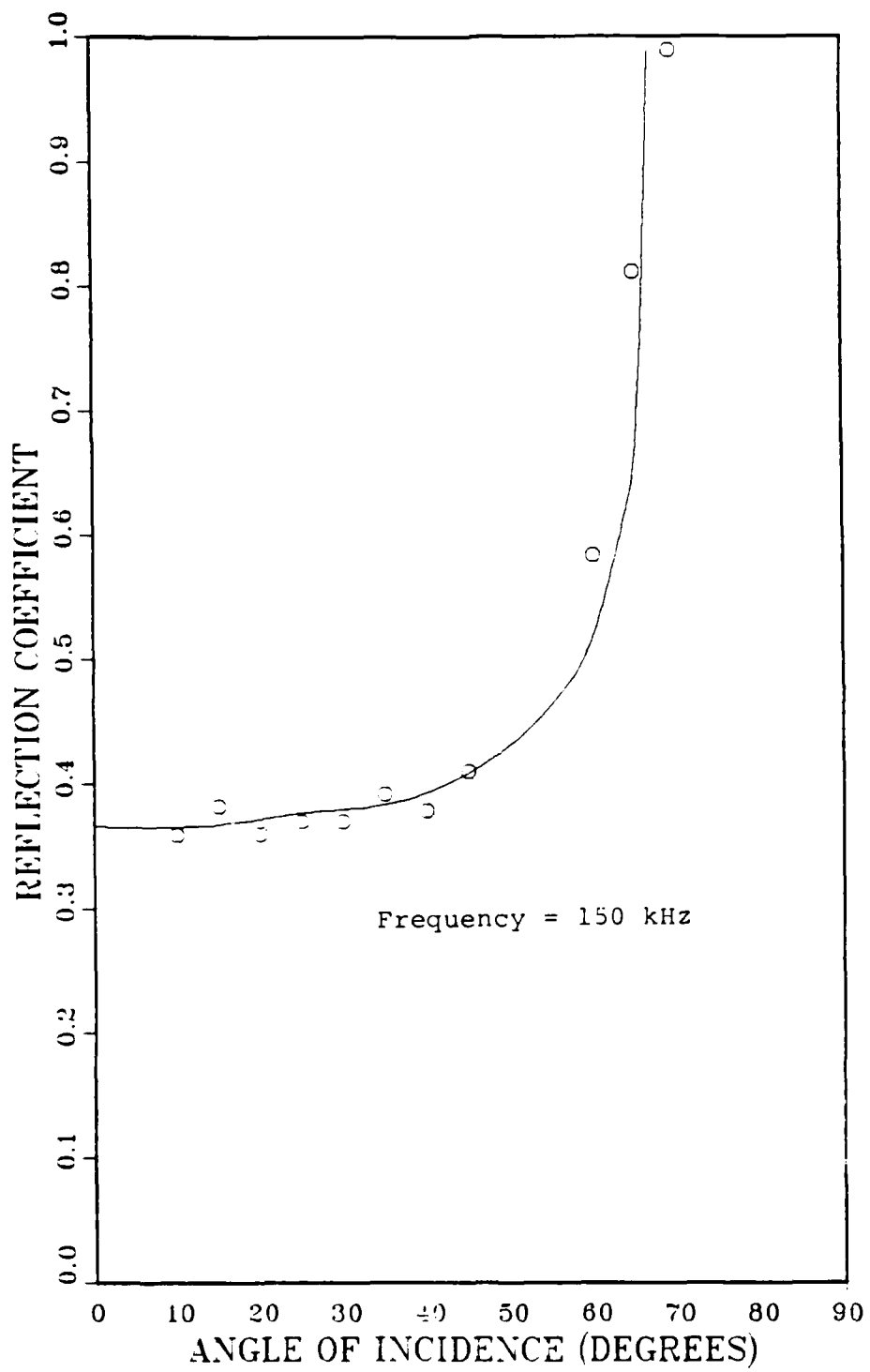


Figure 7. Level Bottom Reflection Coefficients
(o experimental, - predicted)

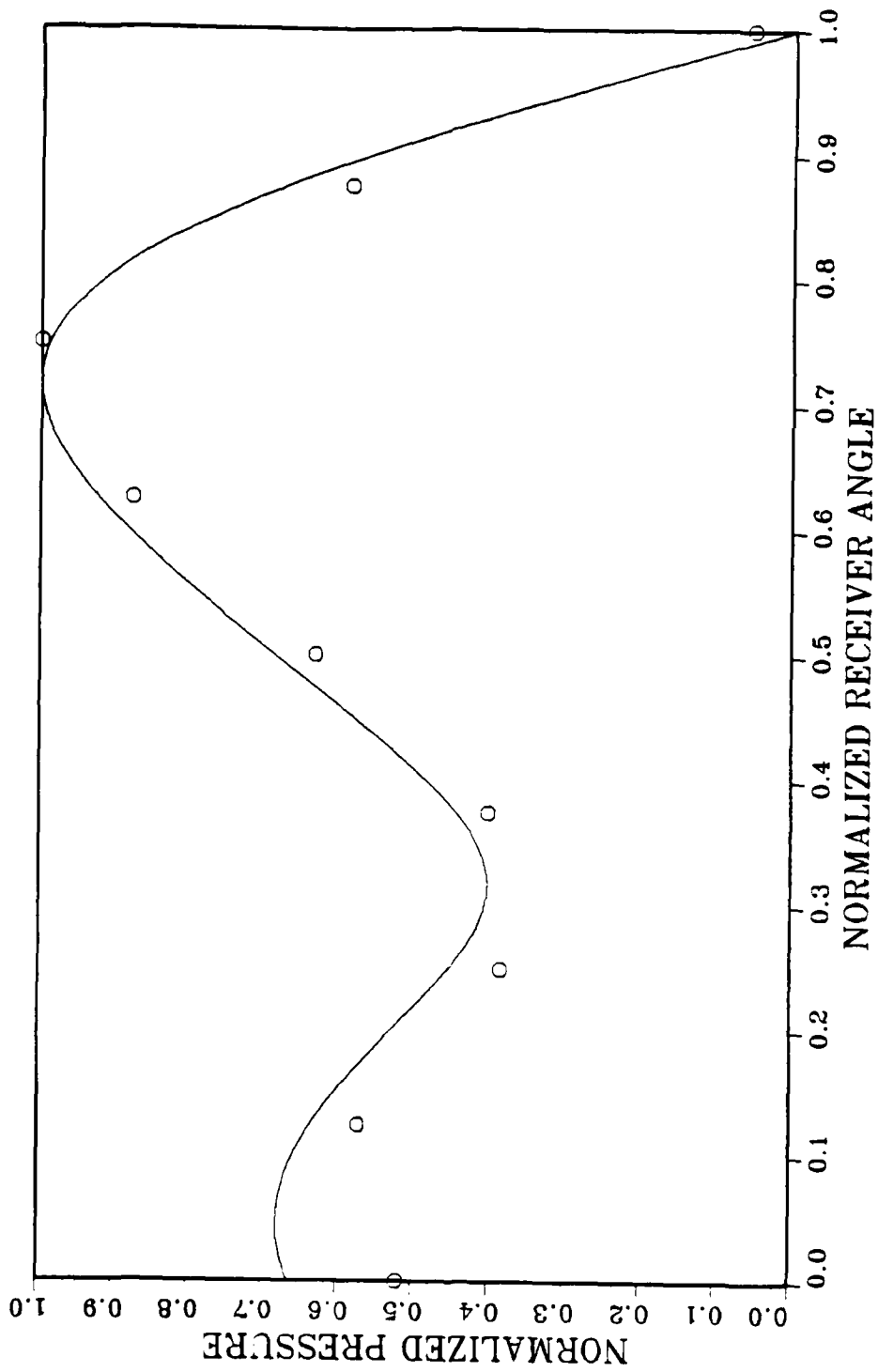


Figure 8. Sound Pressure in the Wedge, $\gamma_0 = 0$, $R_1 = 30$
 $R_2 = 3$ (O experimental, - predicted)

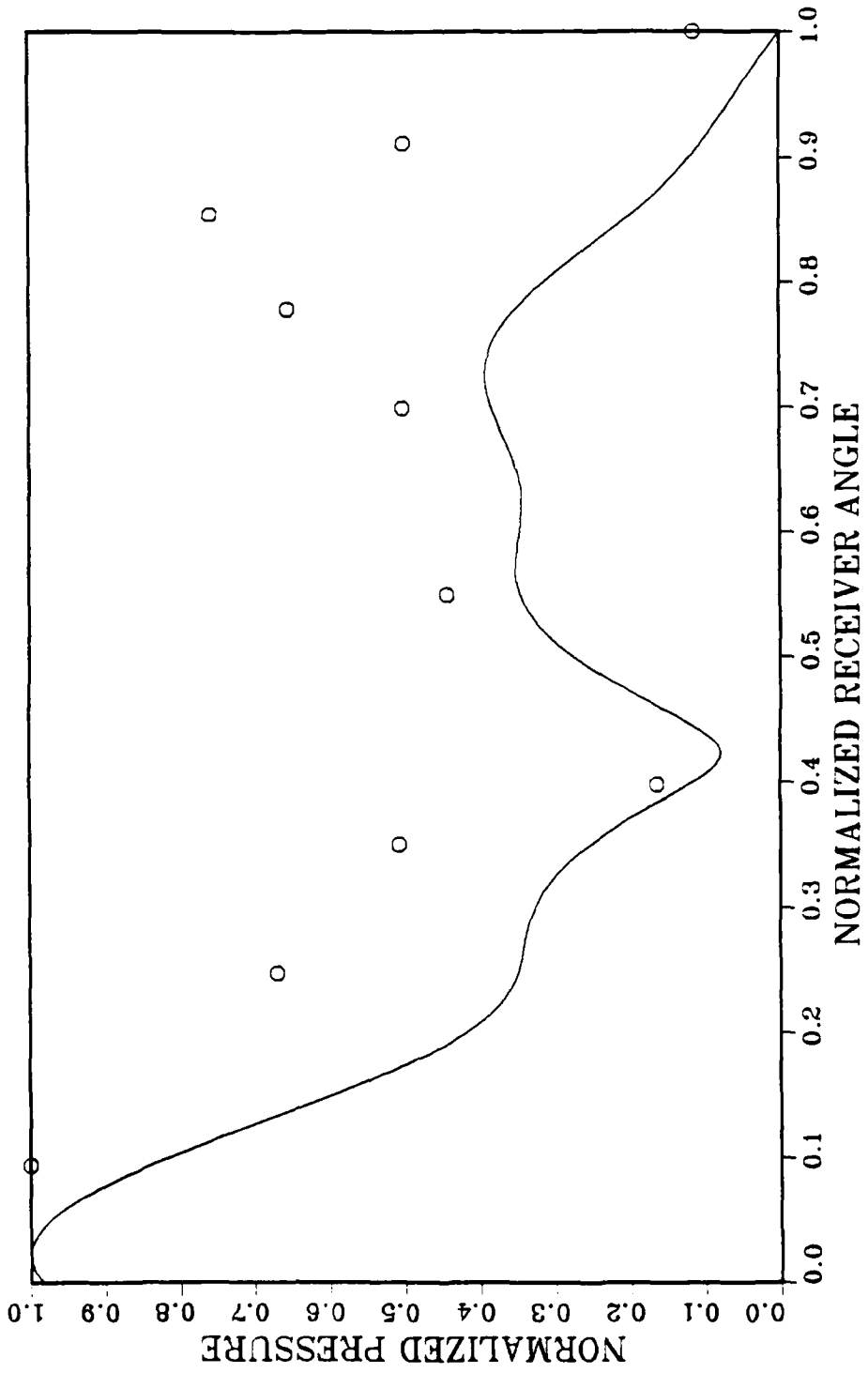


Figure 9. Sound Pressure in the Wedge, $\gamma_0 = 0$, $R_1 = 30$, $R_2 = 5$
 (O experimental, - predicted)

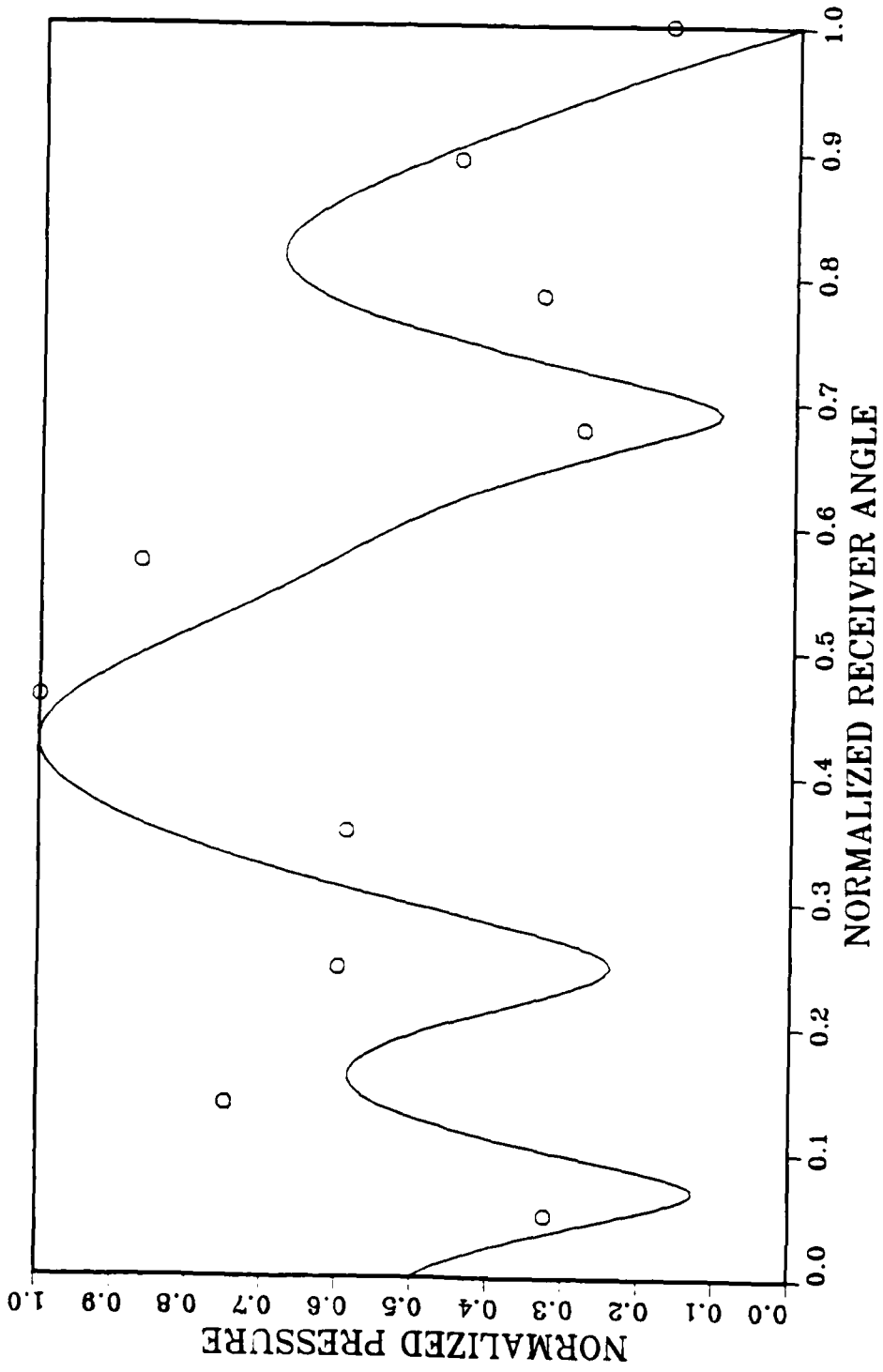


Figure 10. Sound Pressure in the Wedge, $\gamma_0 = 0$, $R_1 = 30$, $R_2 = 7$
 (0 experimental, - predicted)

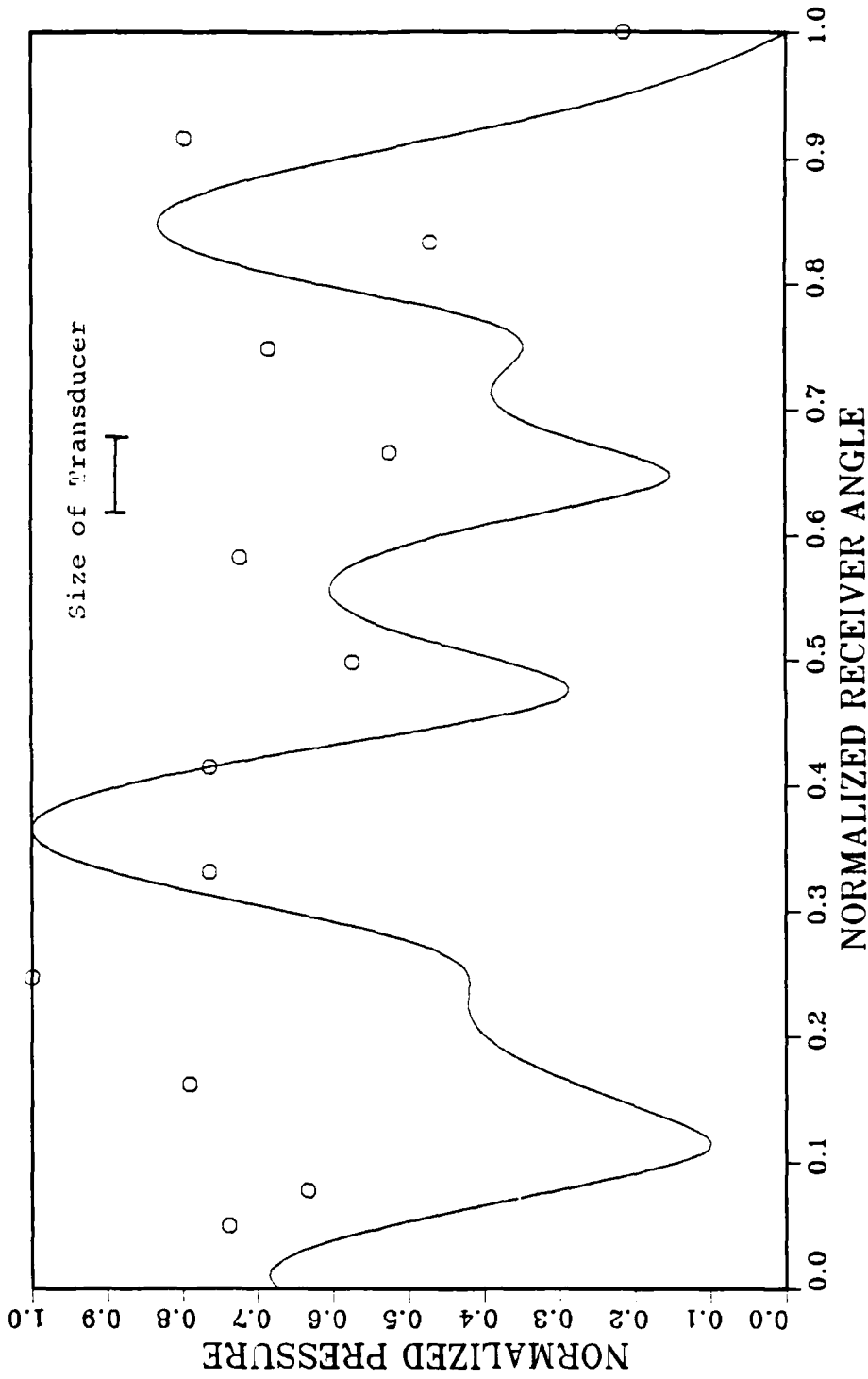


Figure 11. Sound Pressure in the Wedge, $Y_0 = 0$, $R_1 = 30$, $R_2 = 9$
 (O experimental, - predicted)

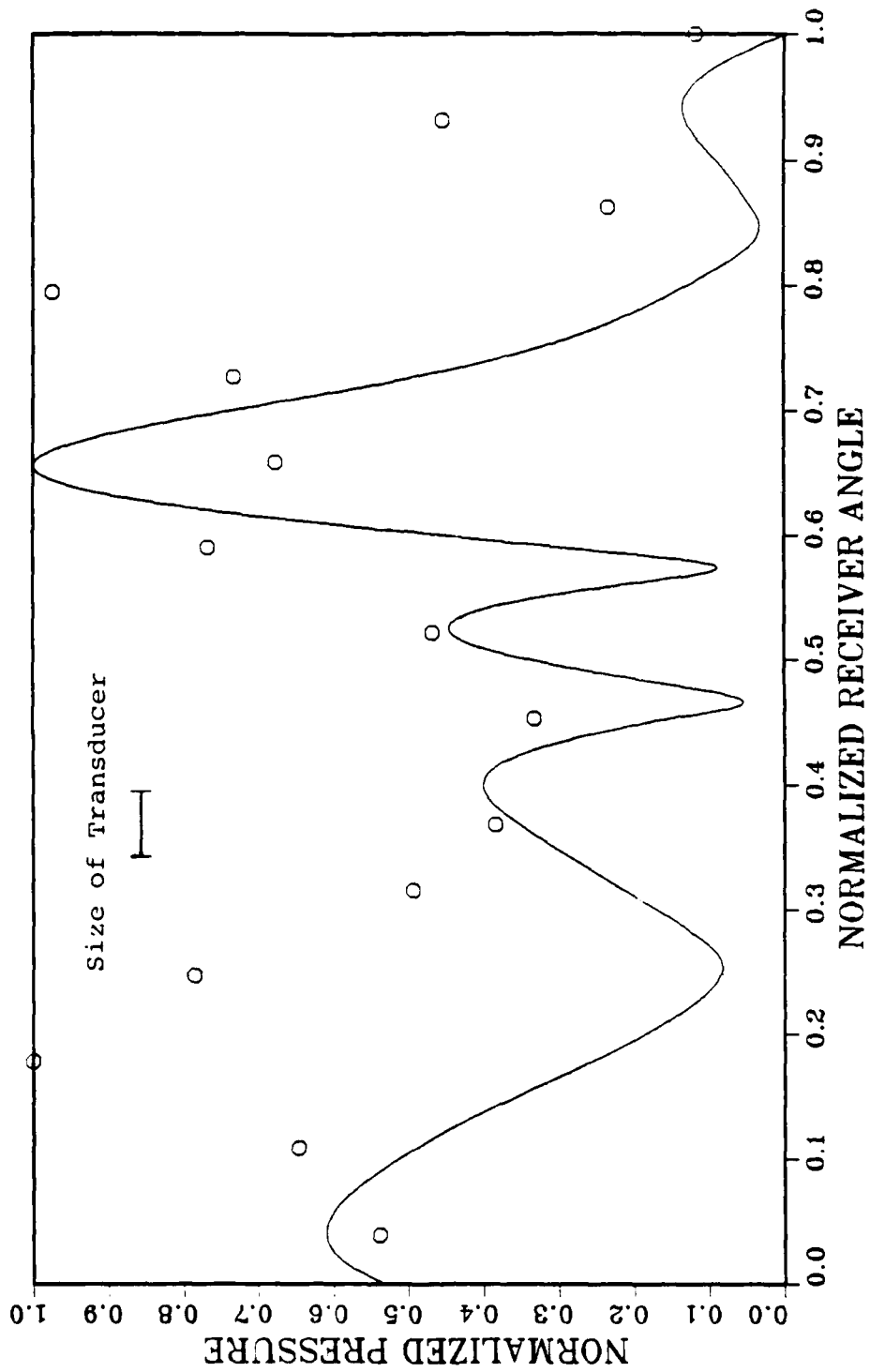


Figure 12. Sound Pressure in the Wedge, $Y_0 = 0$, $R_1 = 30$, $R_2 = 11$
 (O experimental, - predicted)

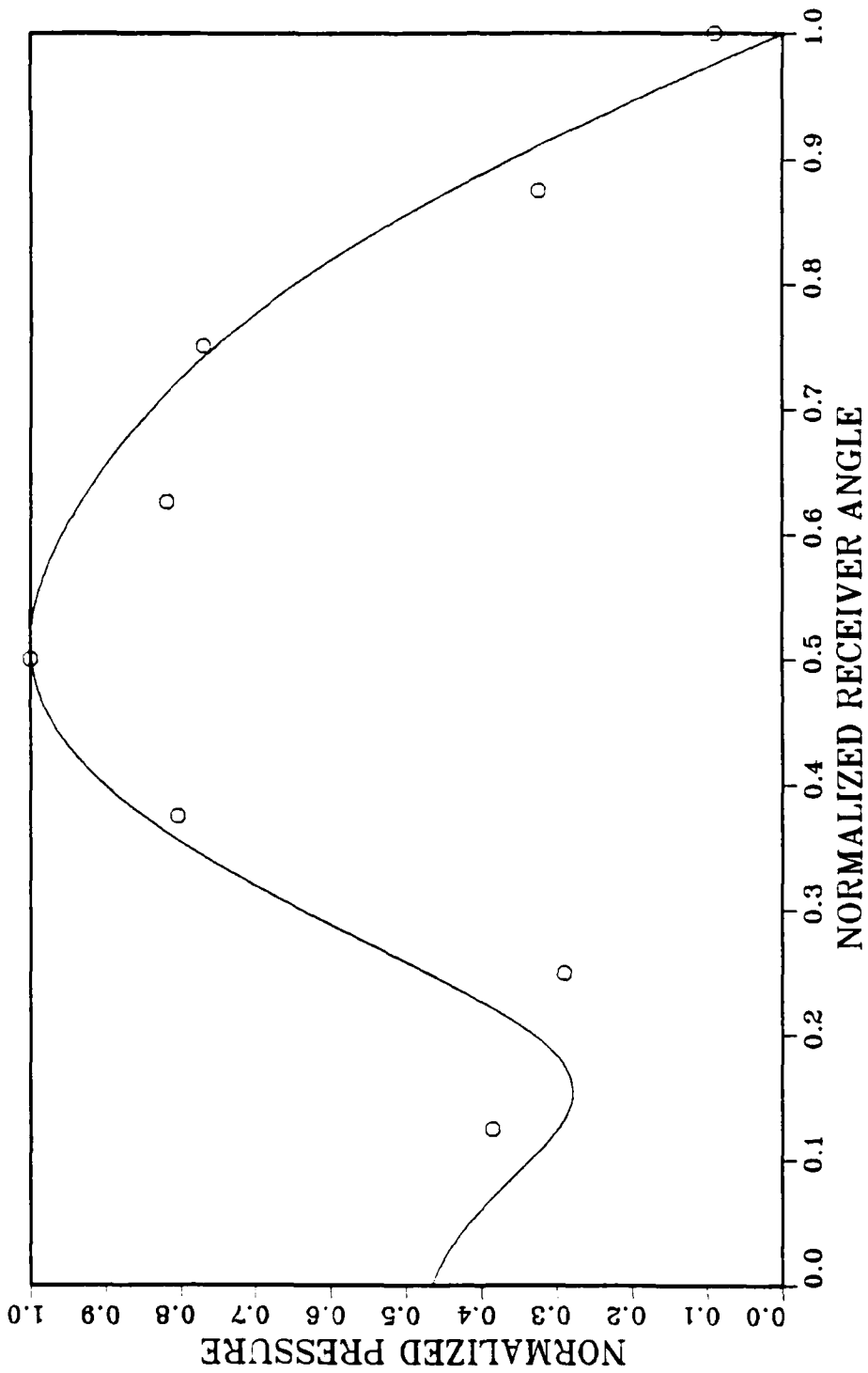


Figure 13. Sound Pressure in the Wedge, $\gamma_0 = 10$, $R_1 = 30$, $F_2 = 3$
 (O experimental, - predicted)

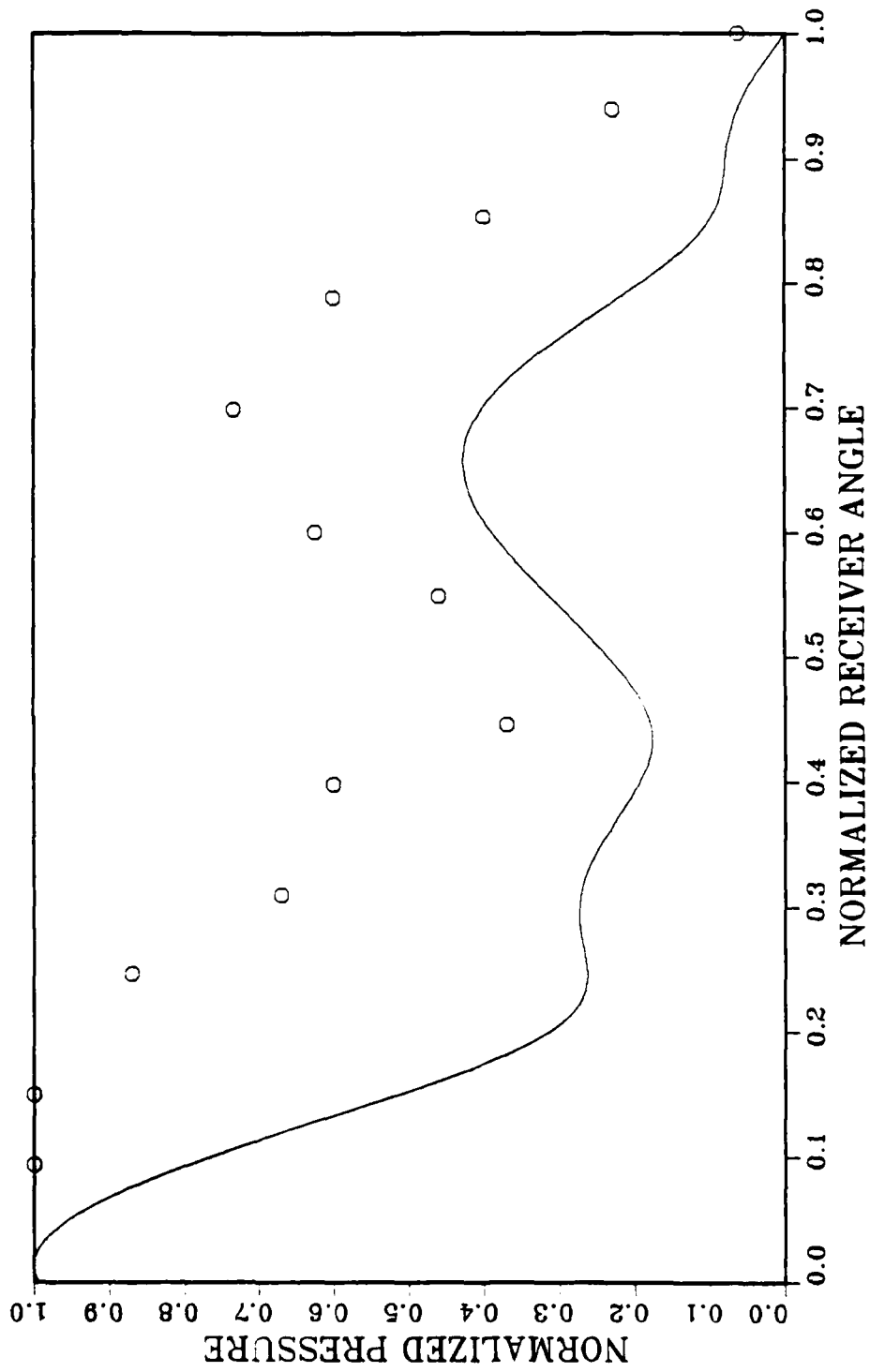


Figure 14. Sound Pressure in the wedge, $\gamma_0 = 10$, $R_1 = 30$, $R_2 = 5$
 (O experimental, - predicted)

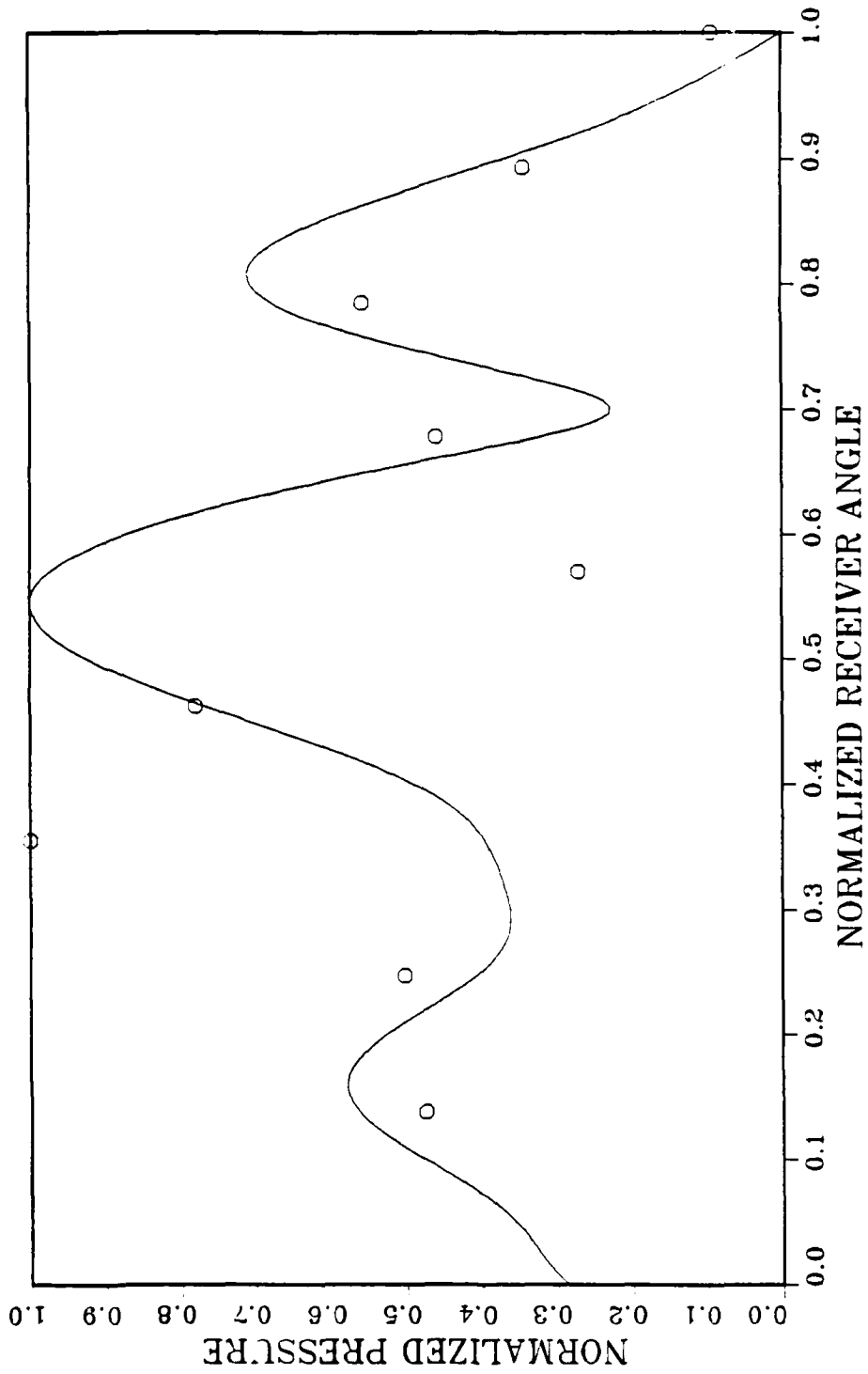


Figure 15. Sound pressure in the Wedge, $\gamma_0 = 10$, $R_1 = 30$, $R_2 = 7$
 (O experimental, - predicted)

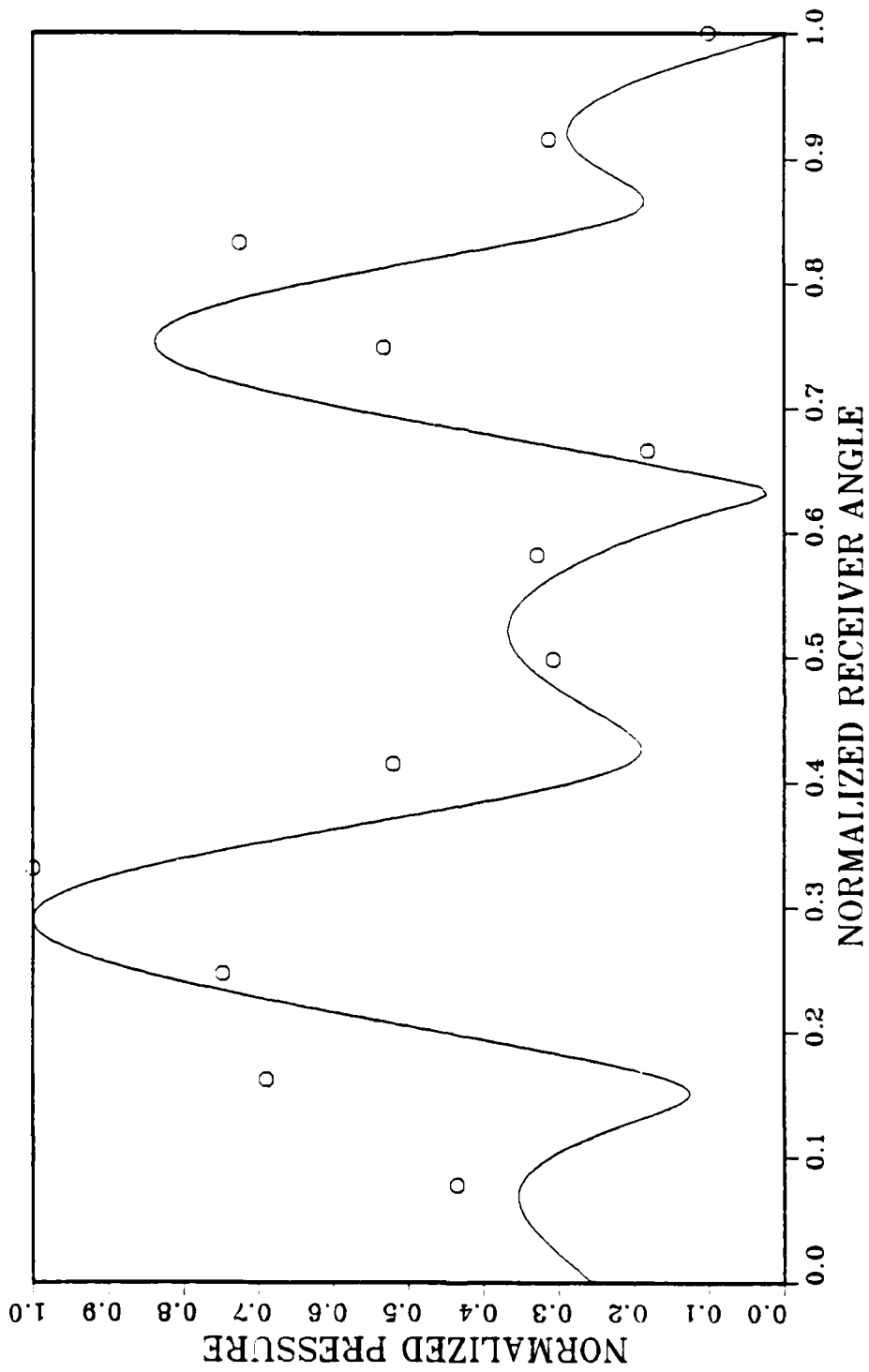


Figure 16. Sound Pressure in the Wedge, $Y_0 = 10$, $R_1 = 30$, $R_2 = 9$
 (O experimental, - predicted)

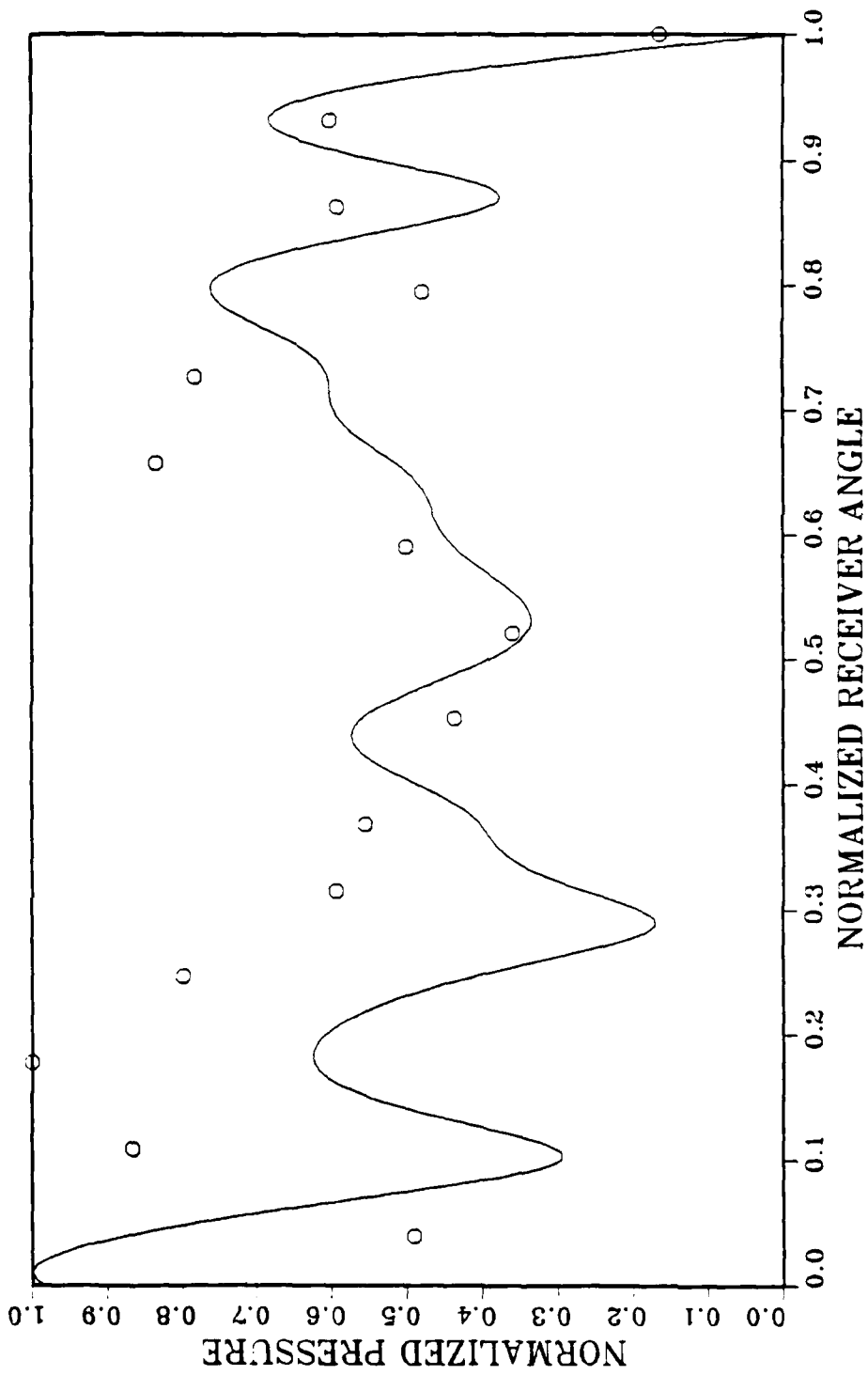


Figure 17. Sound Pressure in the wedge, $Y_0 = 10$, $R_1 = 30$, $R_2 = 11$
 (0 experimental, - predicted)

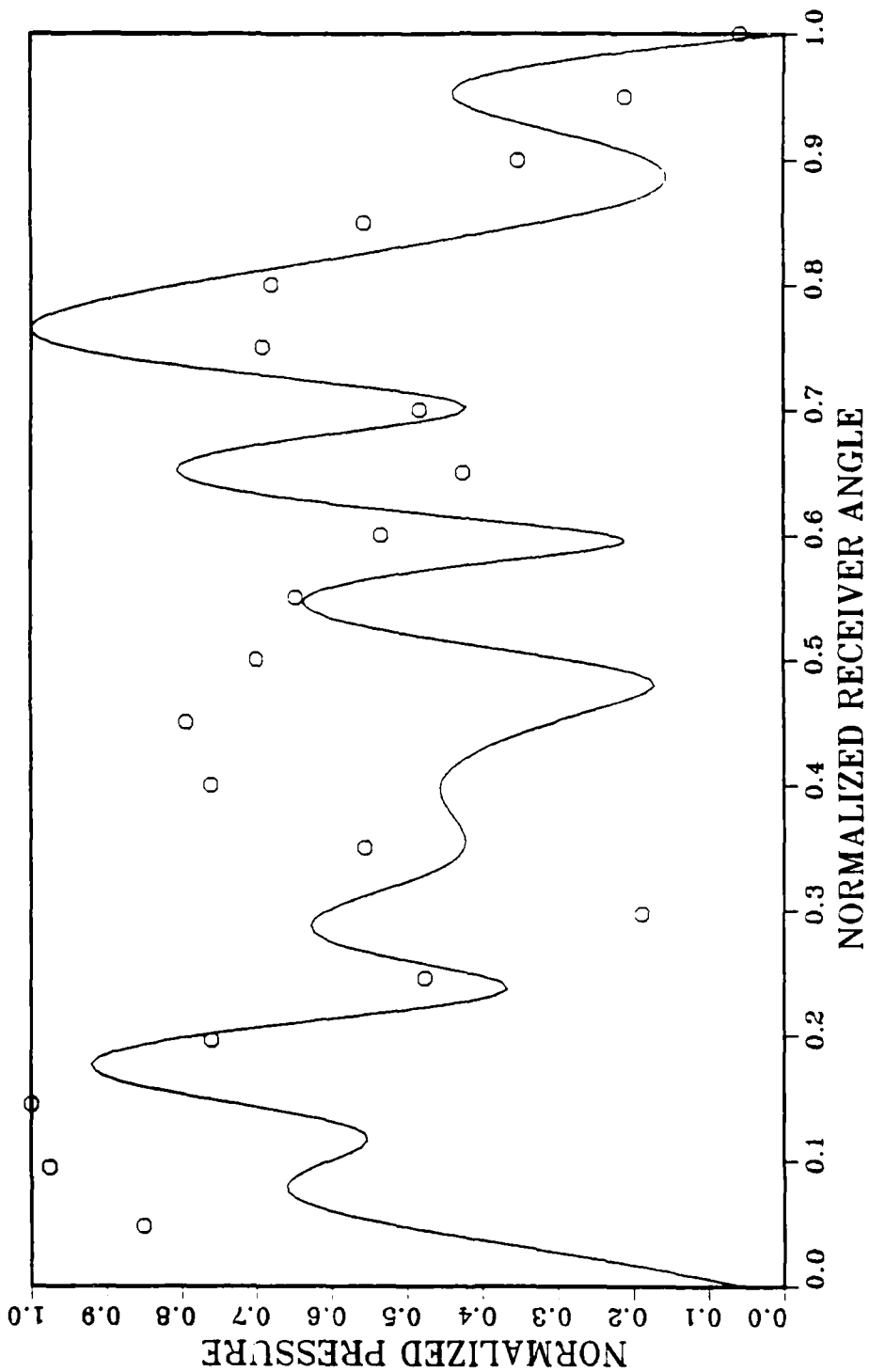


Figure 18. Sound Pressure in the Wedge, $Y_0 = 10$, $R_1 = 30$, $R_2 = 15$
 (0 experimental, - predicted)

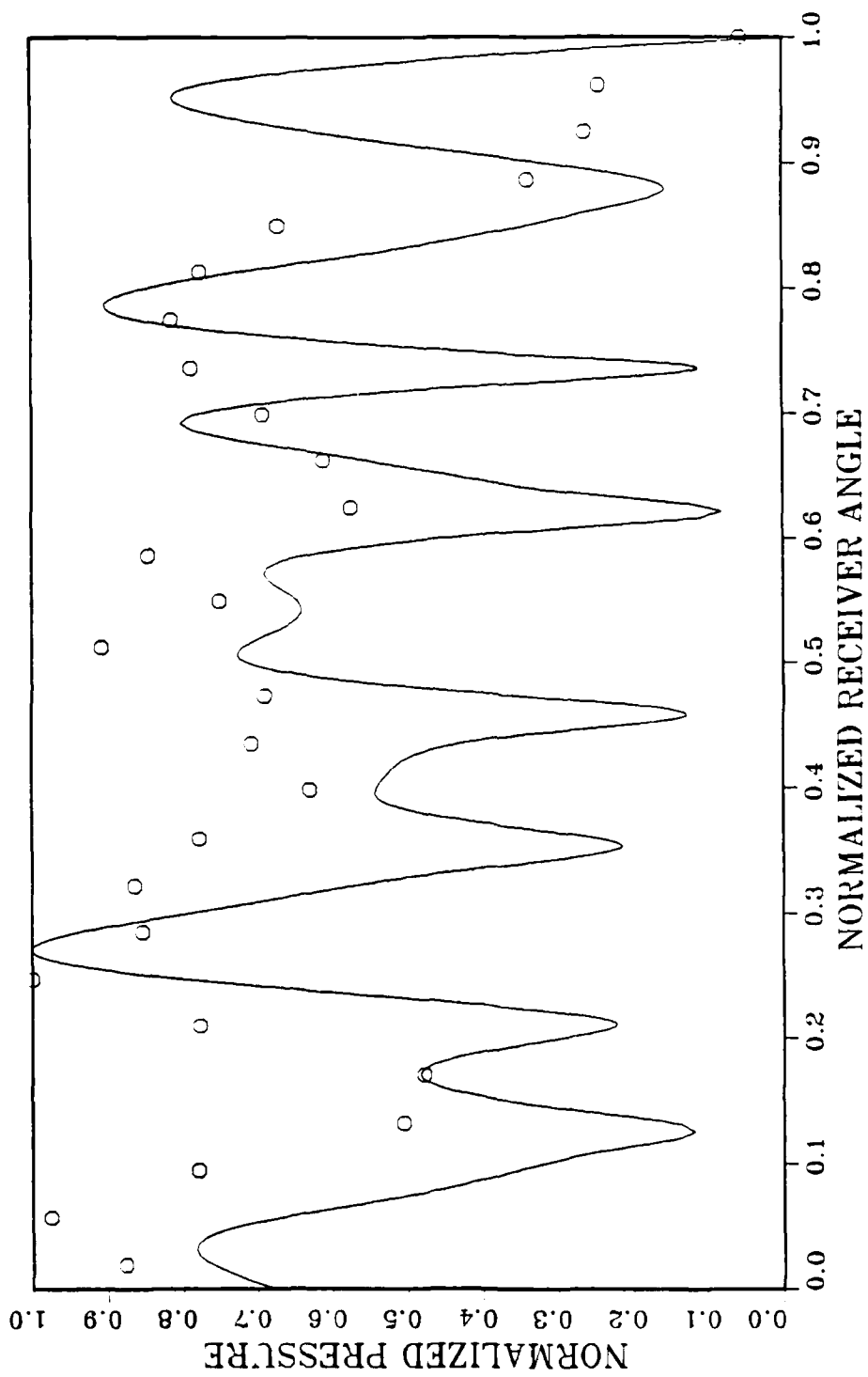


Figure 19. Sound Pressure in the Wedge, $\gamma_0 = 10$, $R_1 = 30$, $R_2 = 20$
 (O experimental, - predicted)

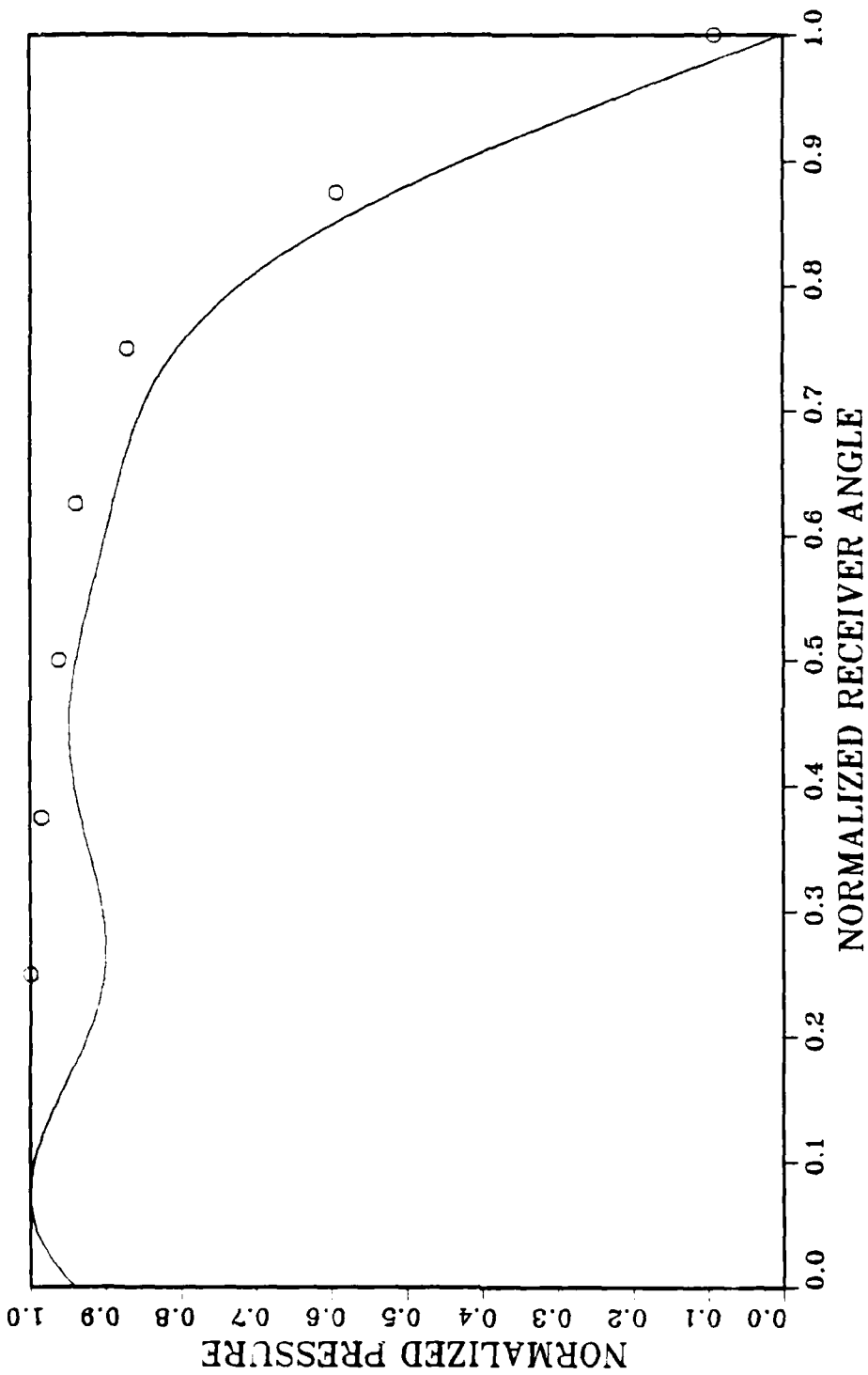


Figure 20. Sound Pressure in the Wedge, $Y_0 = 20$, $R_1 = 30$, $R_2 = 3$
 (O experimental, - predicted)

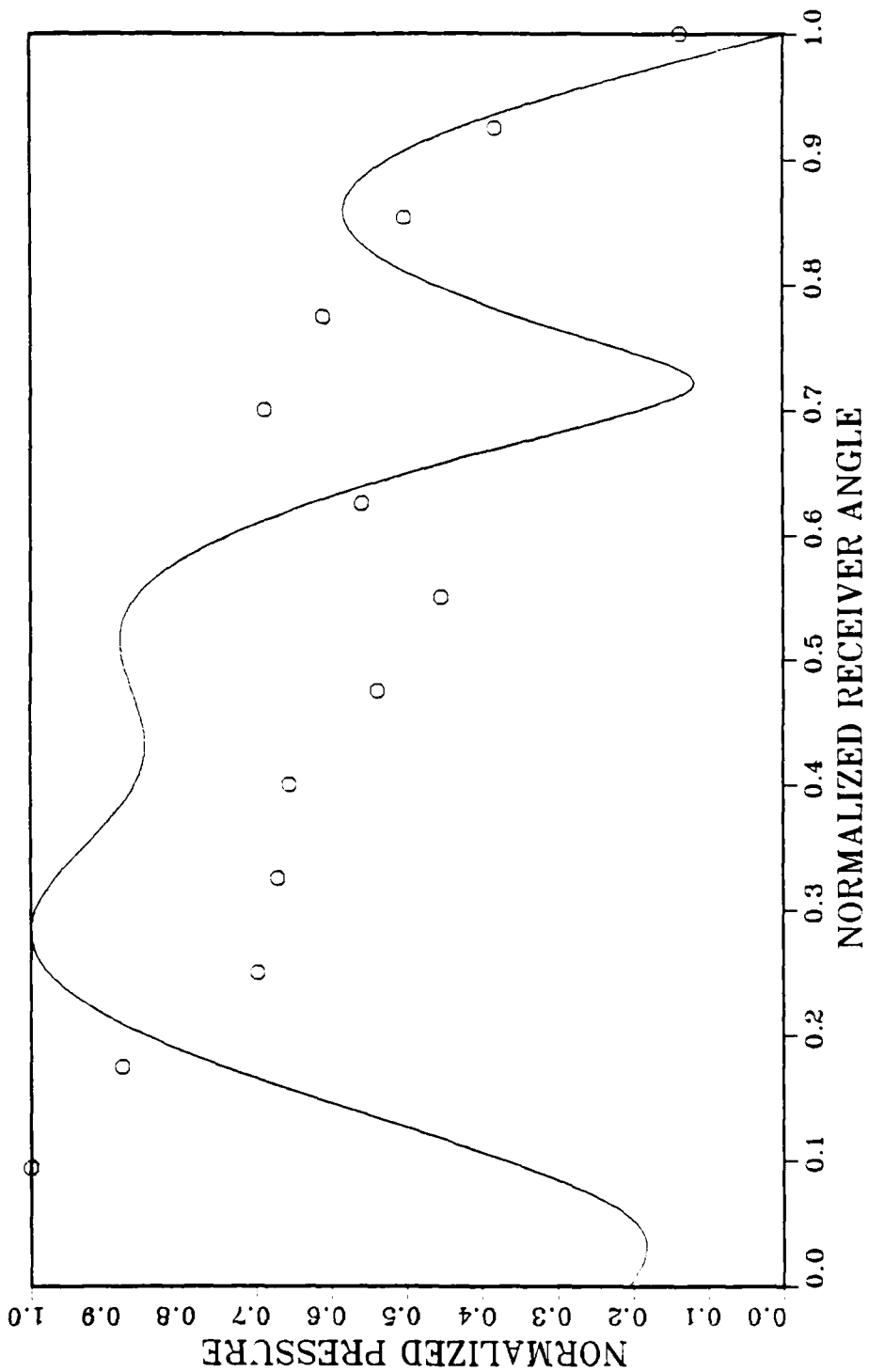


Figure 21. Sound Pressure in the Wedge, $Y_0 = 20$, $R_1 = 30$, $R_2 = 5$
 (0 experimental, - predicted)

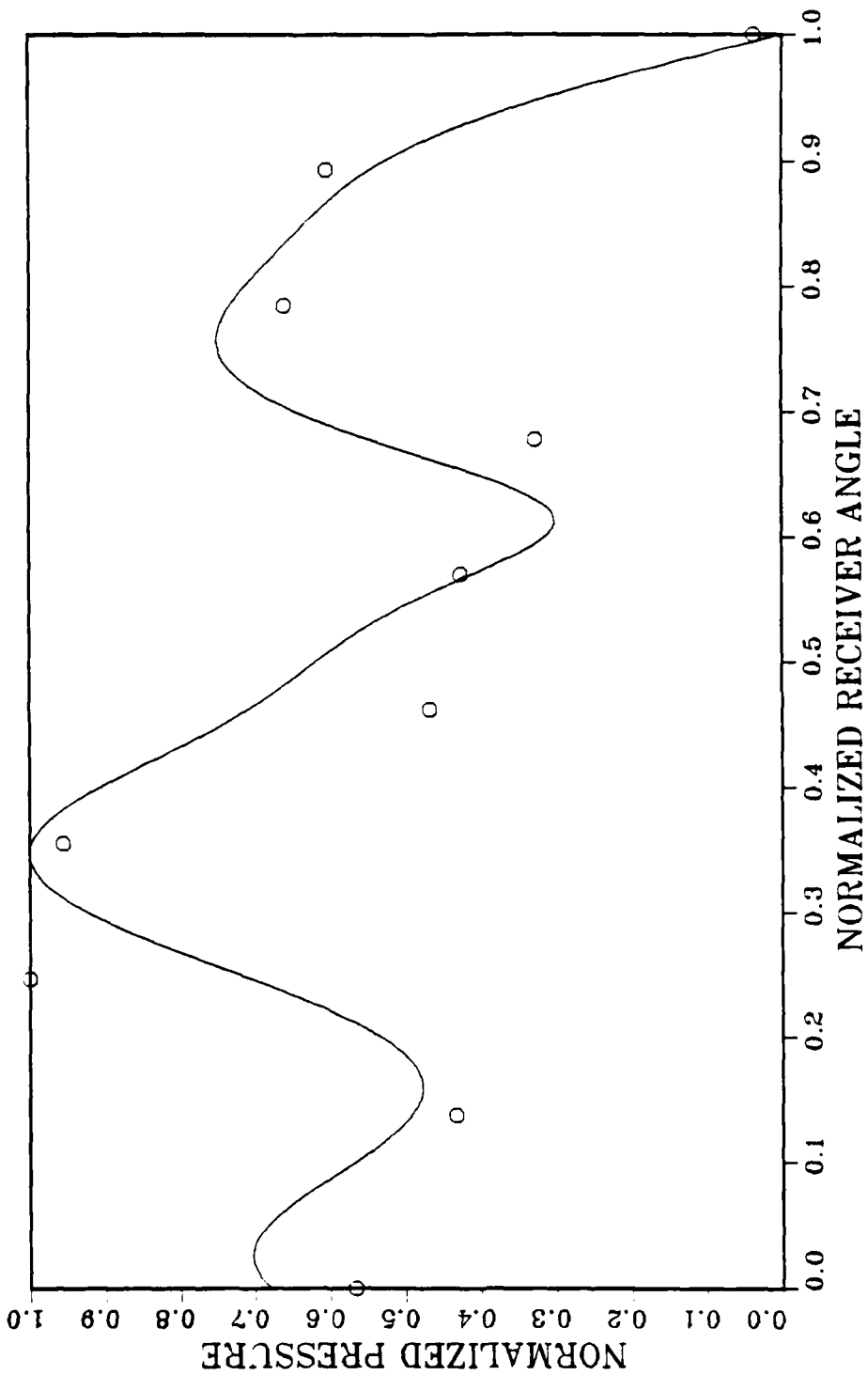


Figure 22. Sound Pressure in the Wedge, $Y_0 = 20$, $R_1 = 30$, $R_2 = 9$
 (O experimental, - predicted)

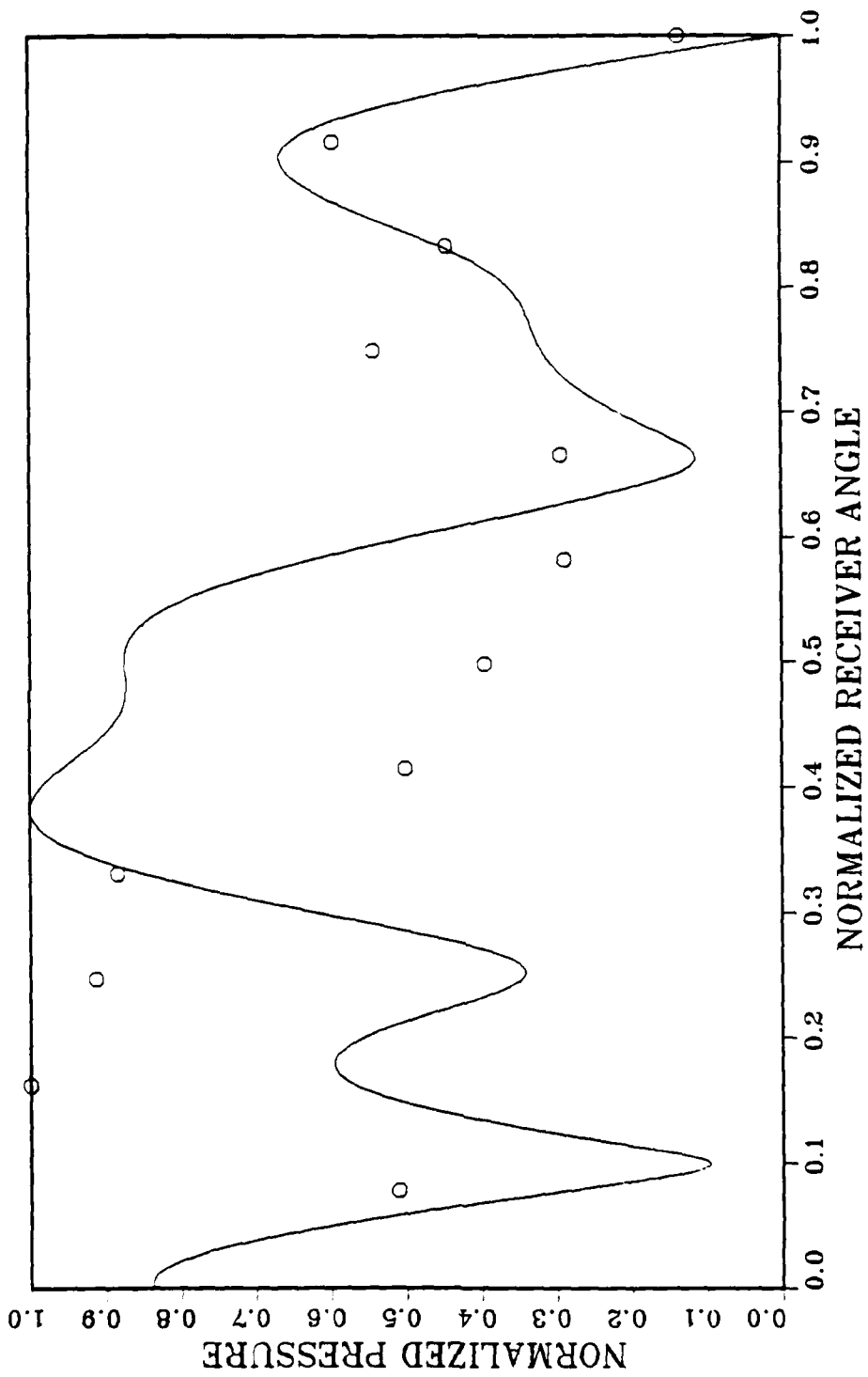


Figure 23. Sound Pressure in the Wedge, $Y_0 = 20$, $R_1 = 30$, $R_2 = 9$
 (O experimental, - predicted)

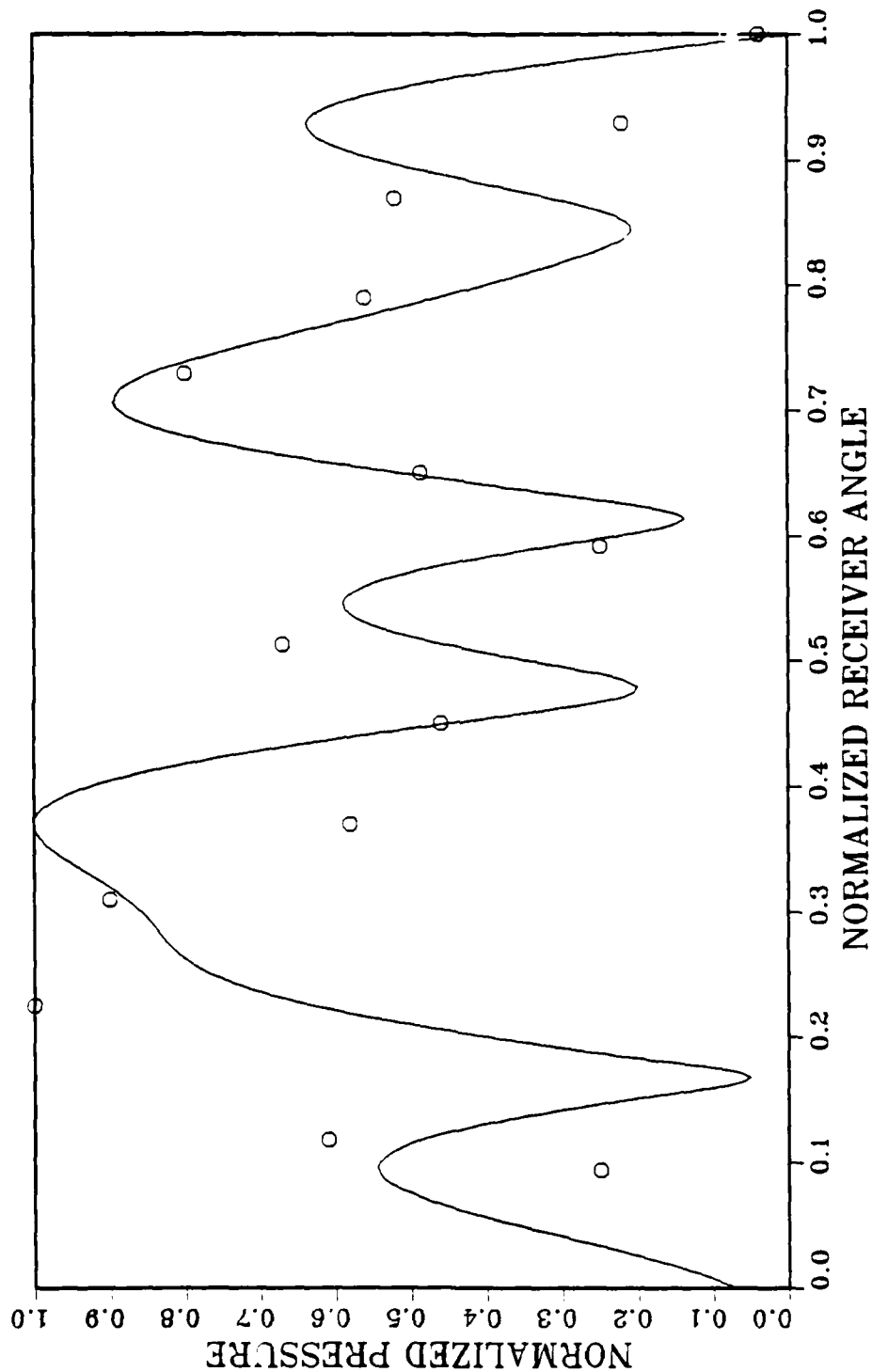


Figure 24. Sound Pressure in the Wedge, $\gamma_0 = 20$, $R_1 = 30$, $R_2 = 11$
 (O experimental, - predicted)

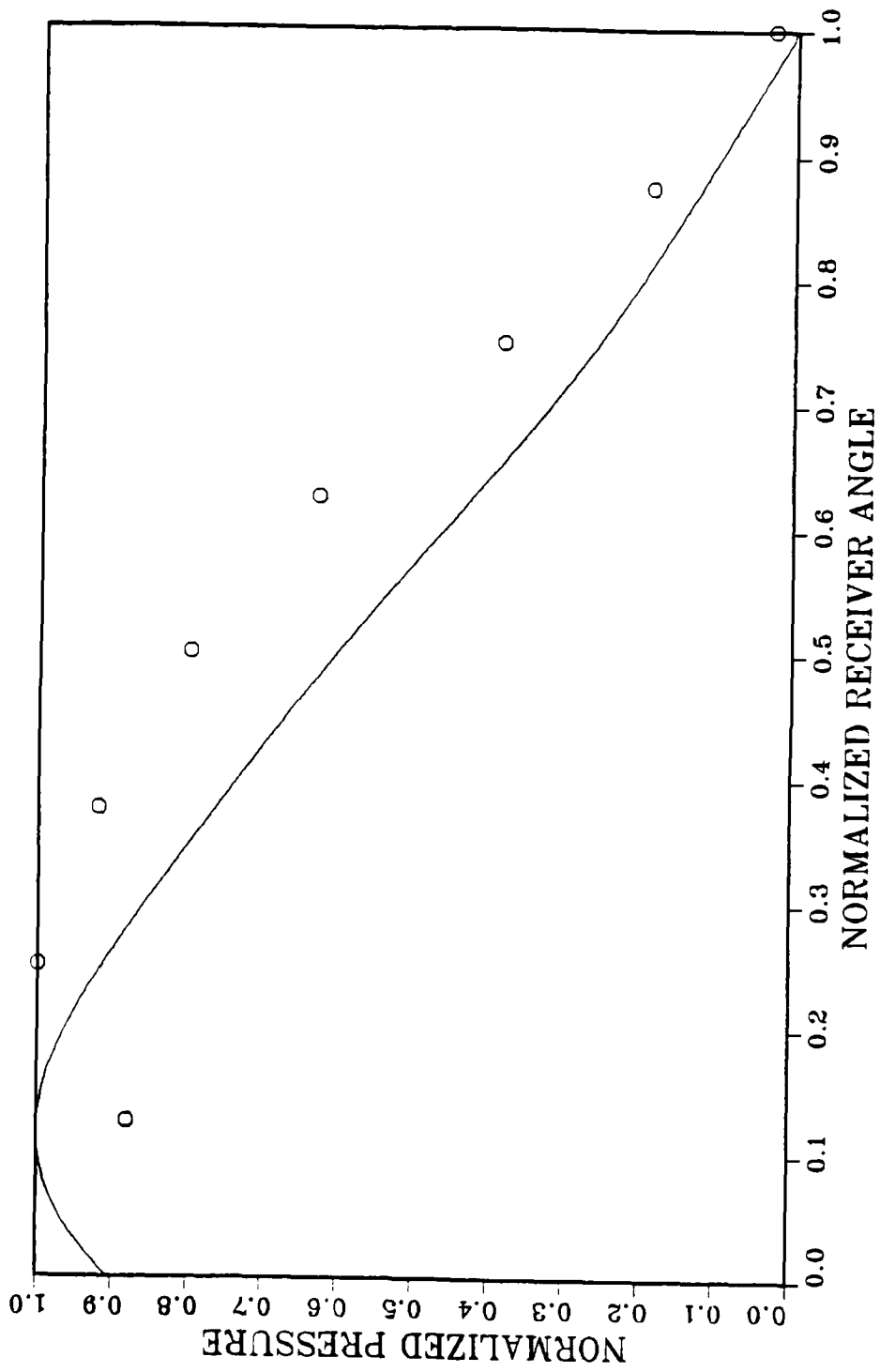


Figure 25. Sound Pressure in the Wedge, $\gamma_0 = 30$, $R_1 = 30$, $R_2 = 3$
 (O experimental, - predicted)

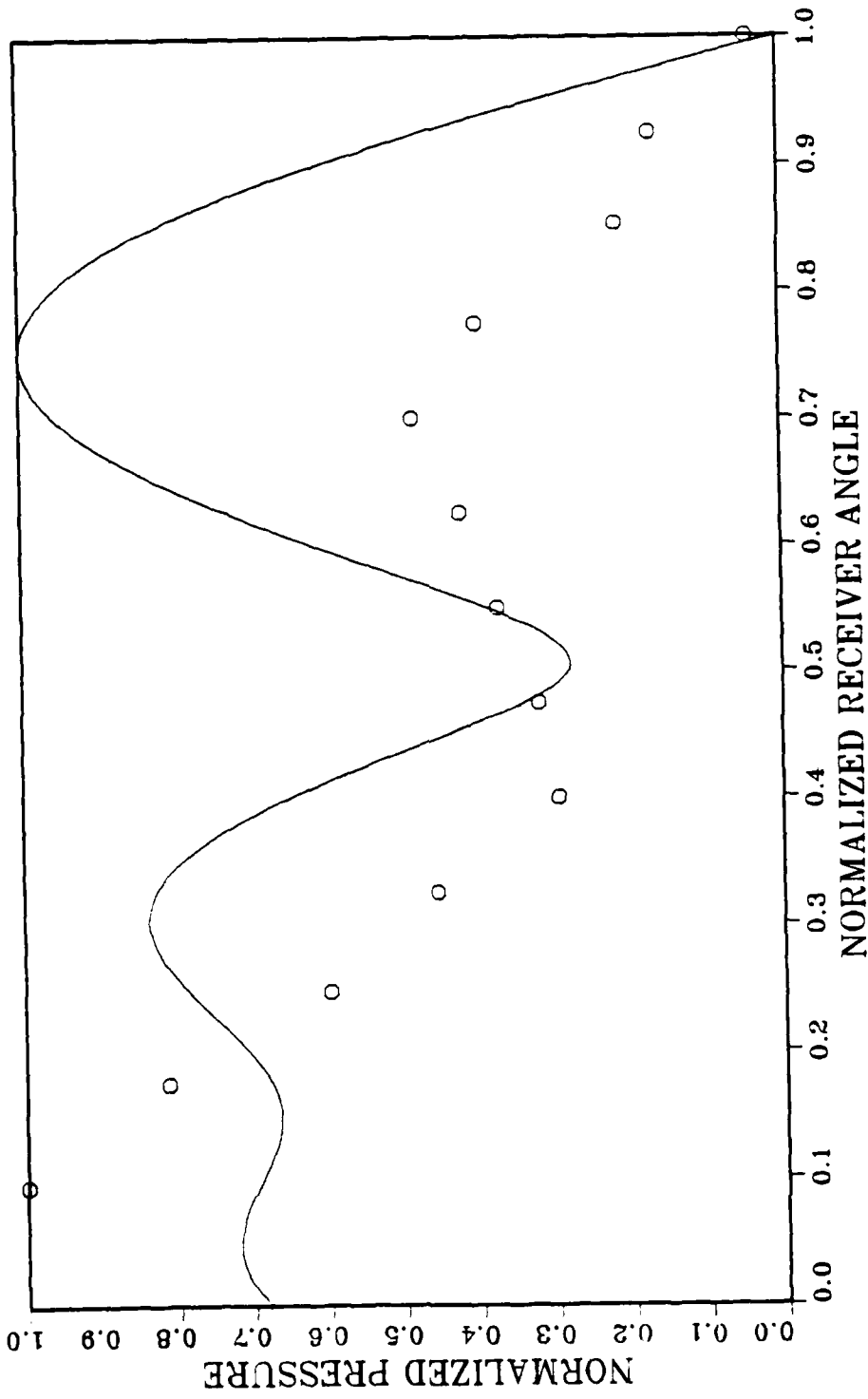


Figure 26. Sound Pressure in the Wedge, $Y_0 = 30$, $R_1 = 30$, $R_2 = 5$
 (O experimental, - predicted)

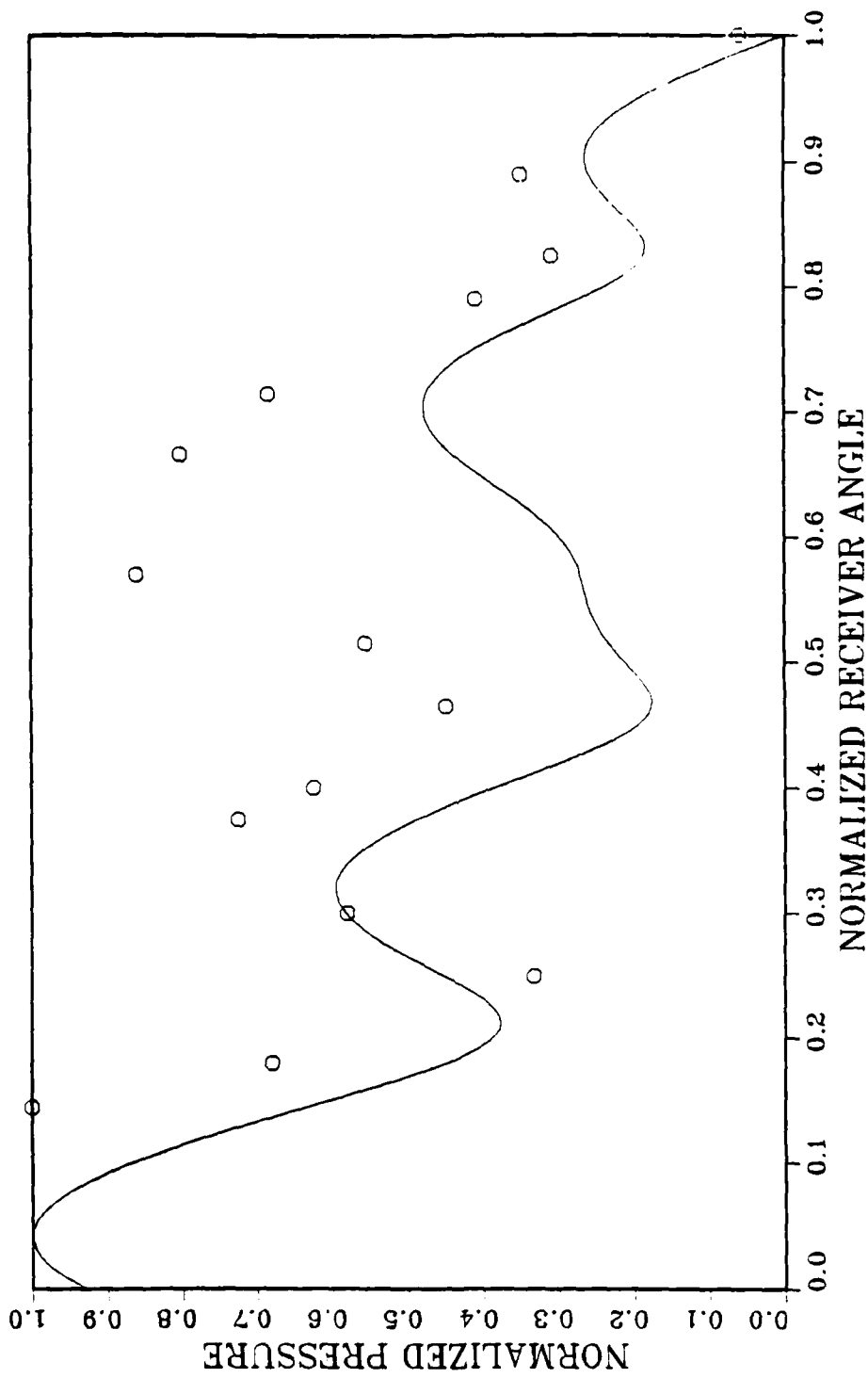


Figure 27. Sound Pressure in the Wedge, $Y_0 = 30$, $P_1 = 30$, $R_2 = 7$
 (O experimental, - predicted)

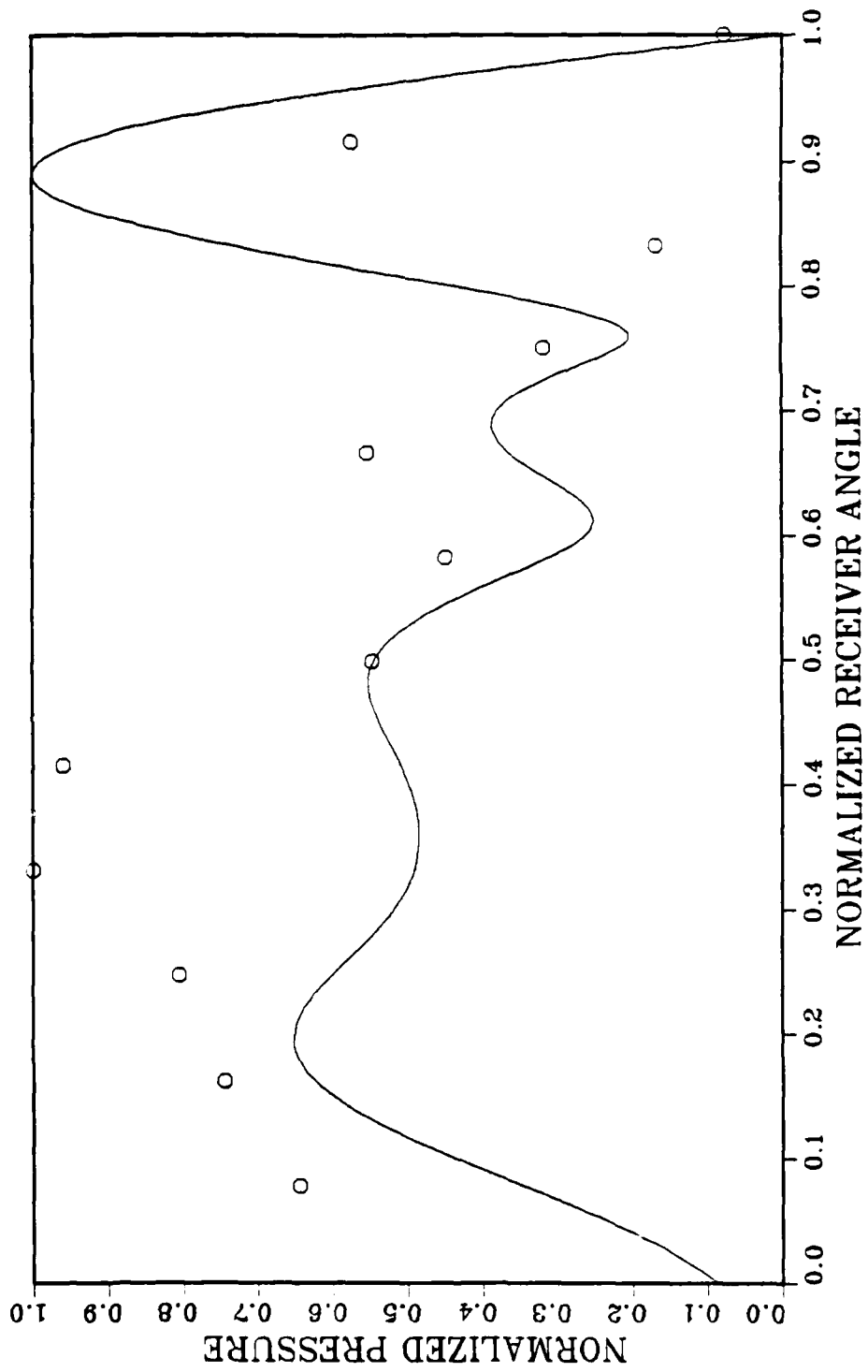


Figure 28. Sound Pressure in the Wedge, $Y_0 = 30$, $R_1 = 30$, $R_2 = 9$
 (O experimental, - predicted)

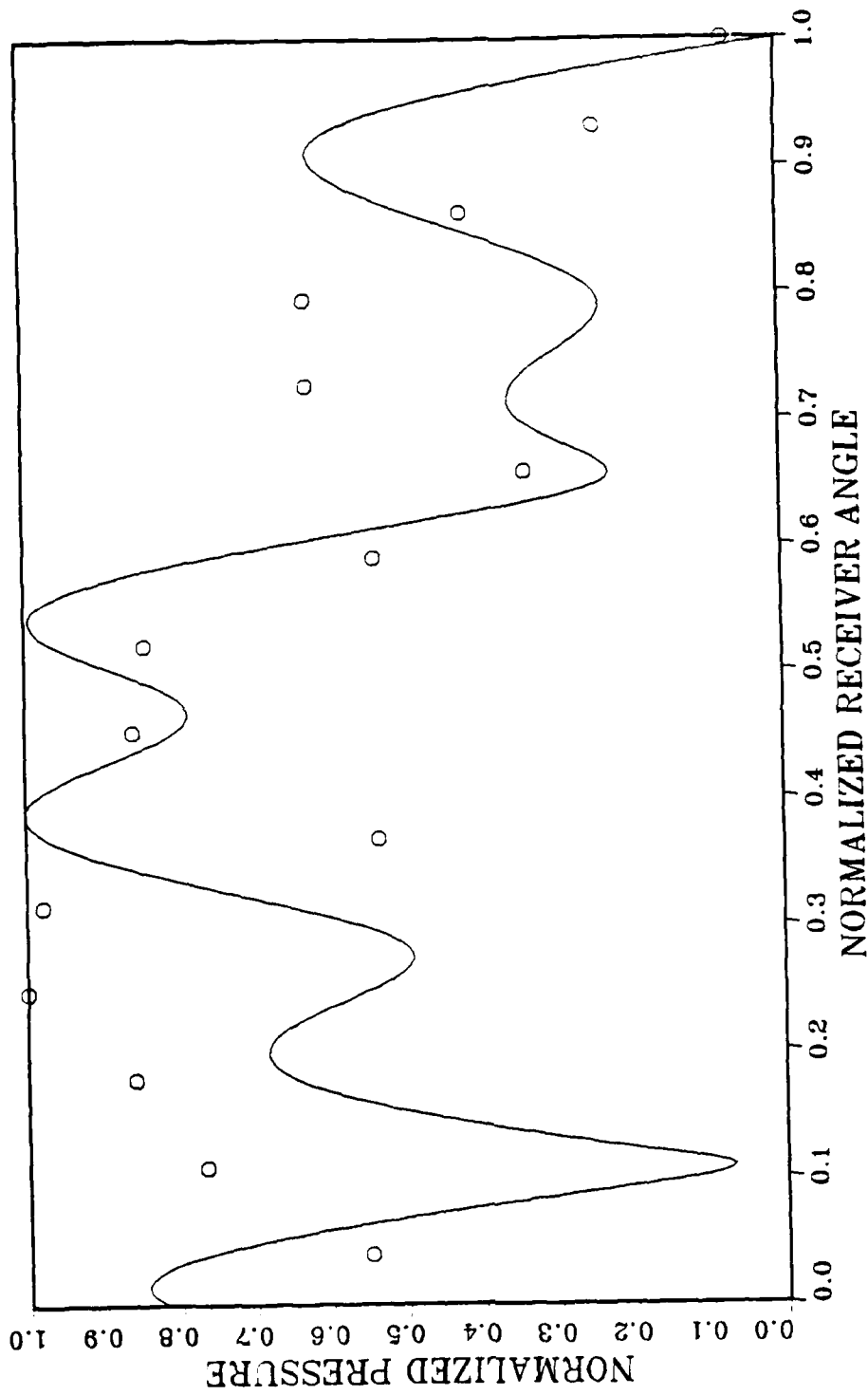


Figure 29. Sound Pressure in the Wedge, $\gamma_0 = 30$, $R_1 = 30$, $R_2 = 11$
 (O experimental, - predicted)

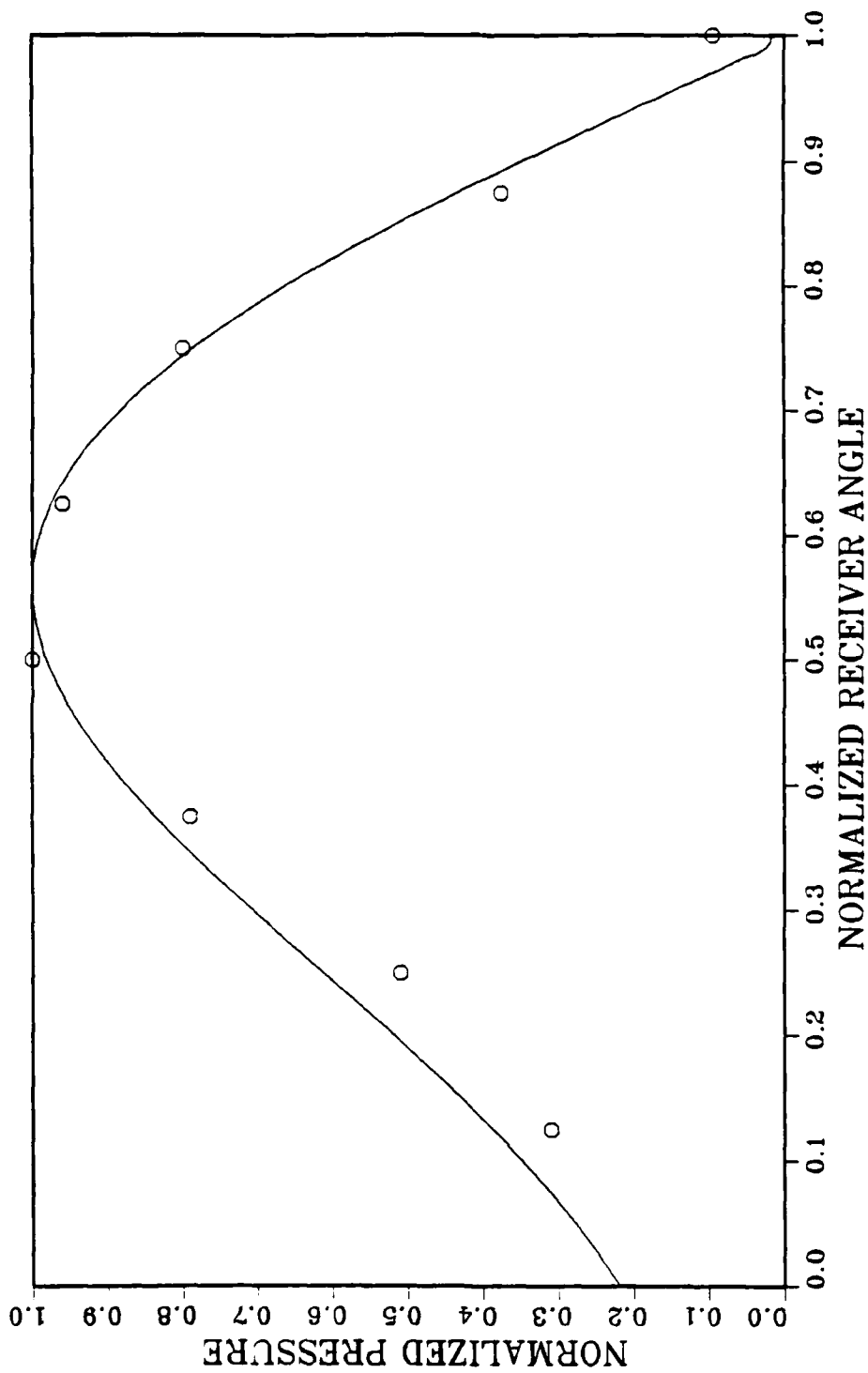


Figure 30. Sound Pressure in the Wedge, $\gamma_0 = 50$, $R_1 = 30$, $R_2 = 3$
 (O experimental, - predicted)

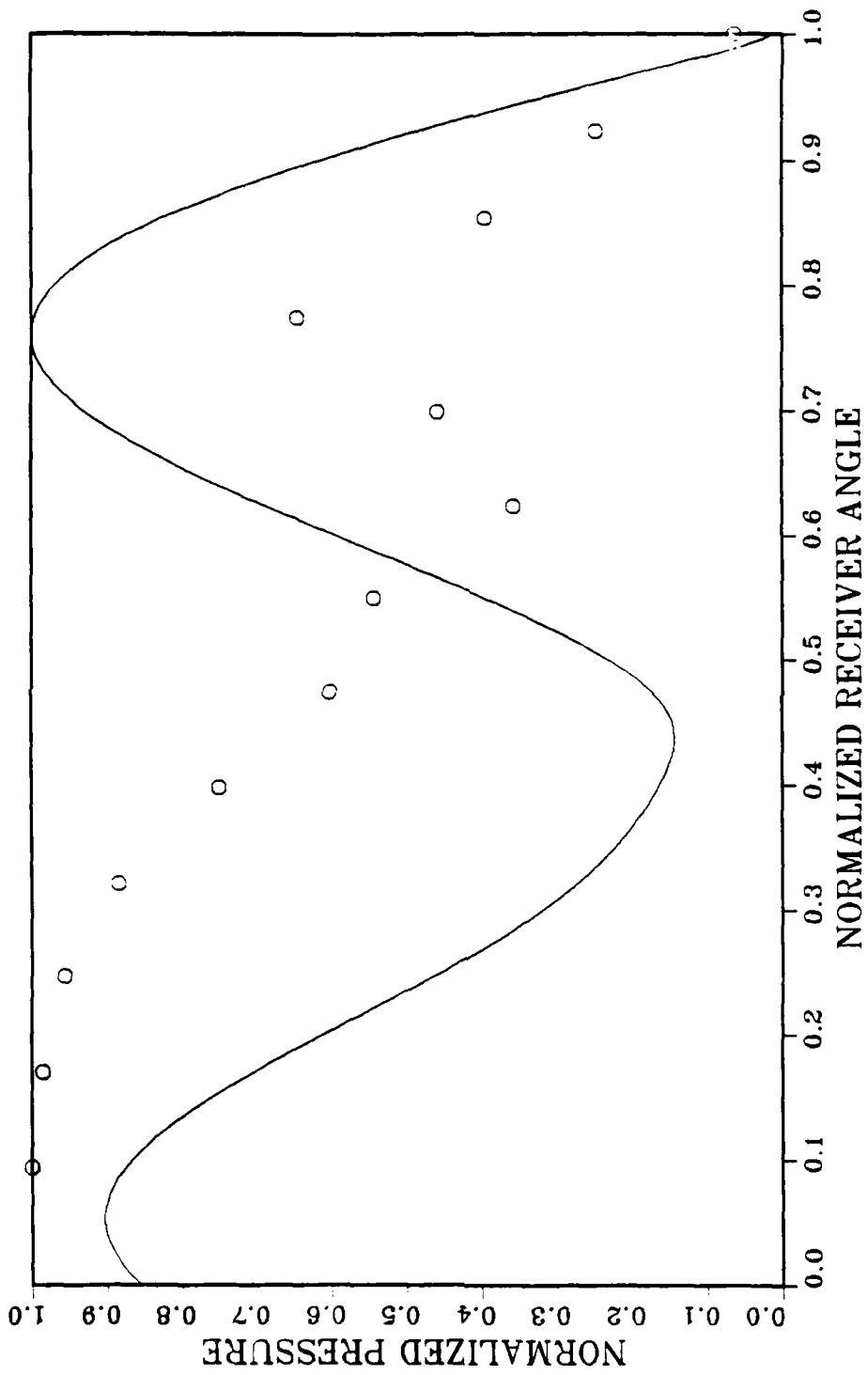


Figure 31. Sound Pressure in the Wedge, $Y_0 = 50$, $R_1 = 30$, $R_2 = 5$
 (O experimental, - predicted)

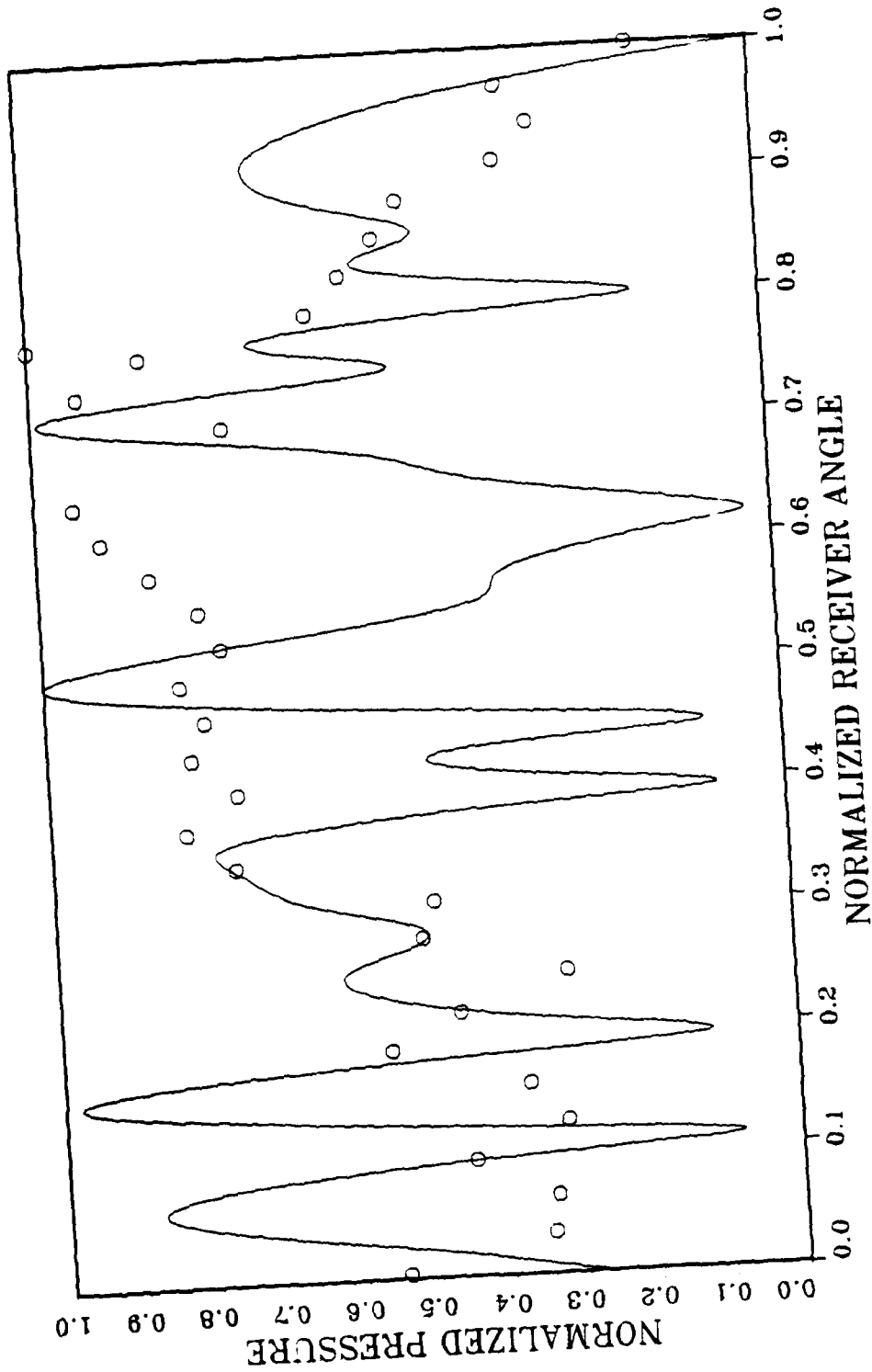


Figure 32. Sound Pressure in the wedge, $Y_0 = 10$, $R_1 = 25$, $R_2 = 25$
 (O experimental, - predicted)

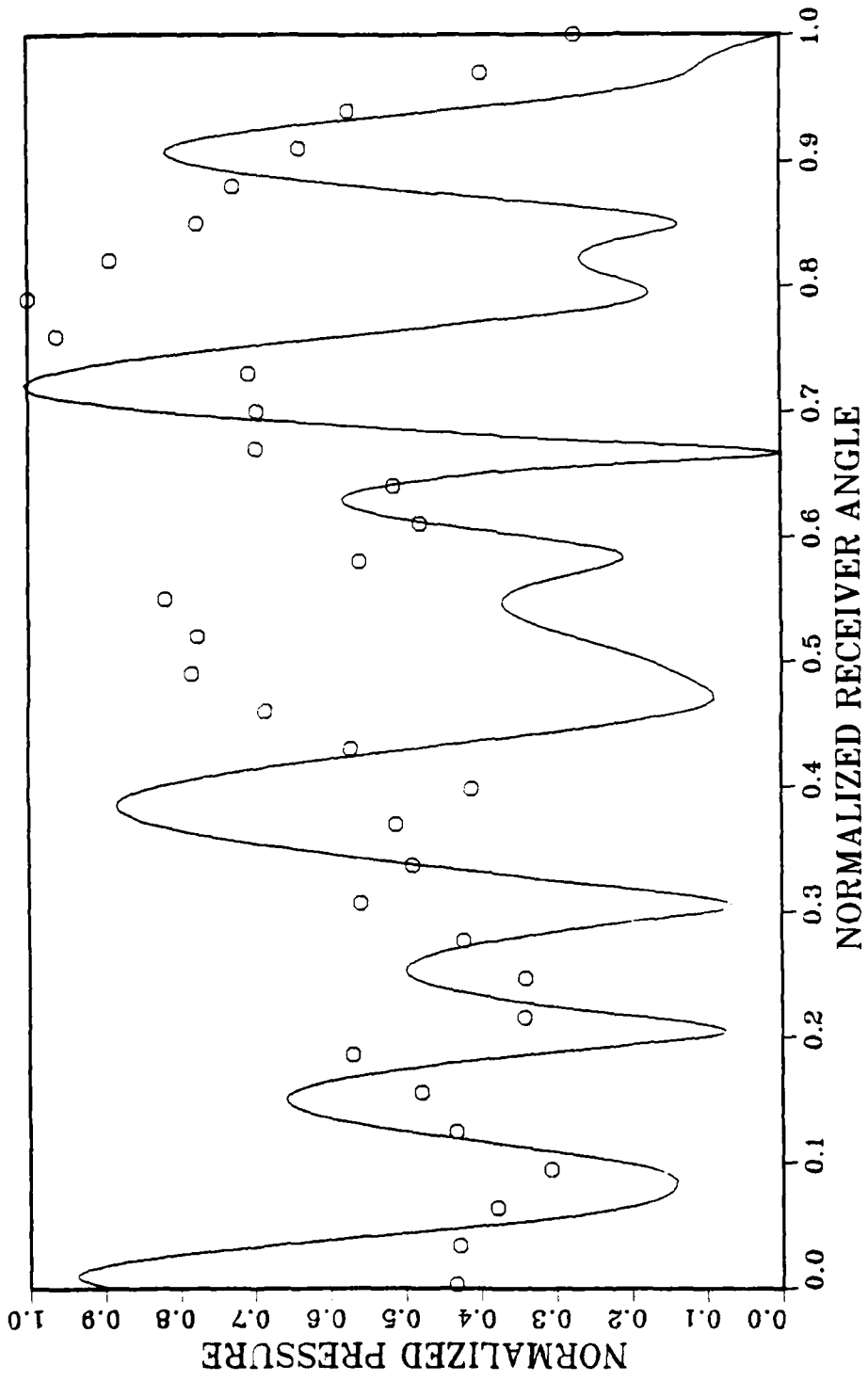


Figure 33. Sound Pressure in the Wedge, $Y_0 = 20$, $R_1 = 25$, $R_2 = 25$
 (0 experimental, - predicted)

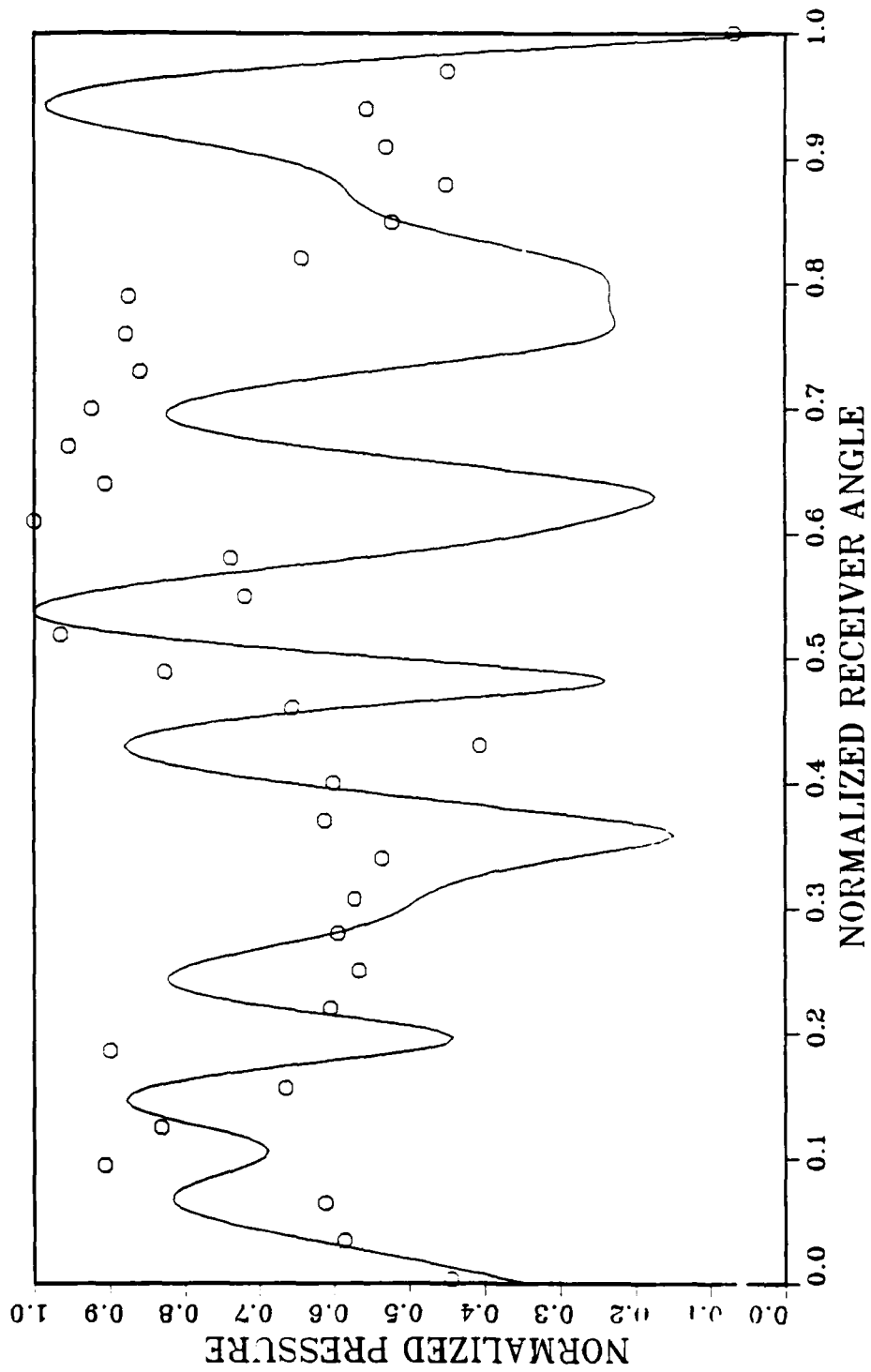


Figure 34. Sound Pressure in the Wedge, $Y_0 = 30$, $R_1 = 25$, $R_2 = 25$
 (O experimental, - predicted)

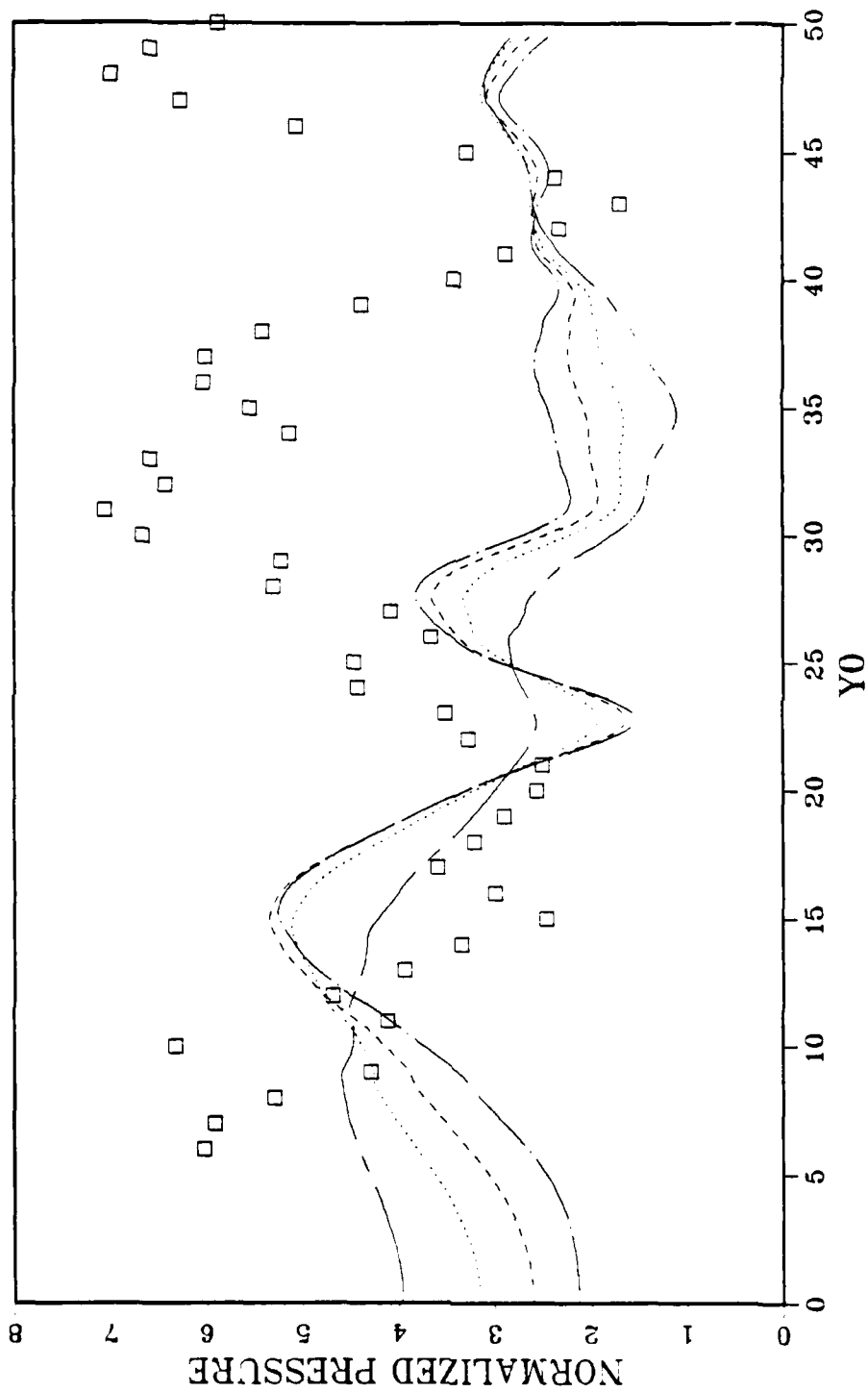


Figure 35. Sound Pressure in the Wedge, $R_2 = 3$, $D = 4.75$
 (□) experimental, ... $D = 4.75$ predicted, - - - $D = 4.25$
 predicted, -.-. $D = 3.75$ predicted, ---- $D = 5.5$ predicted)

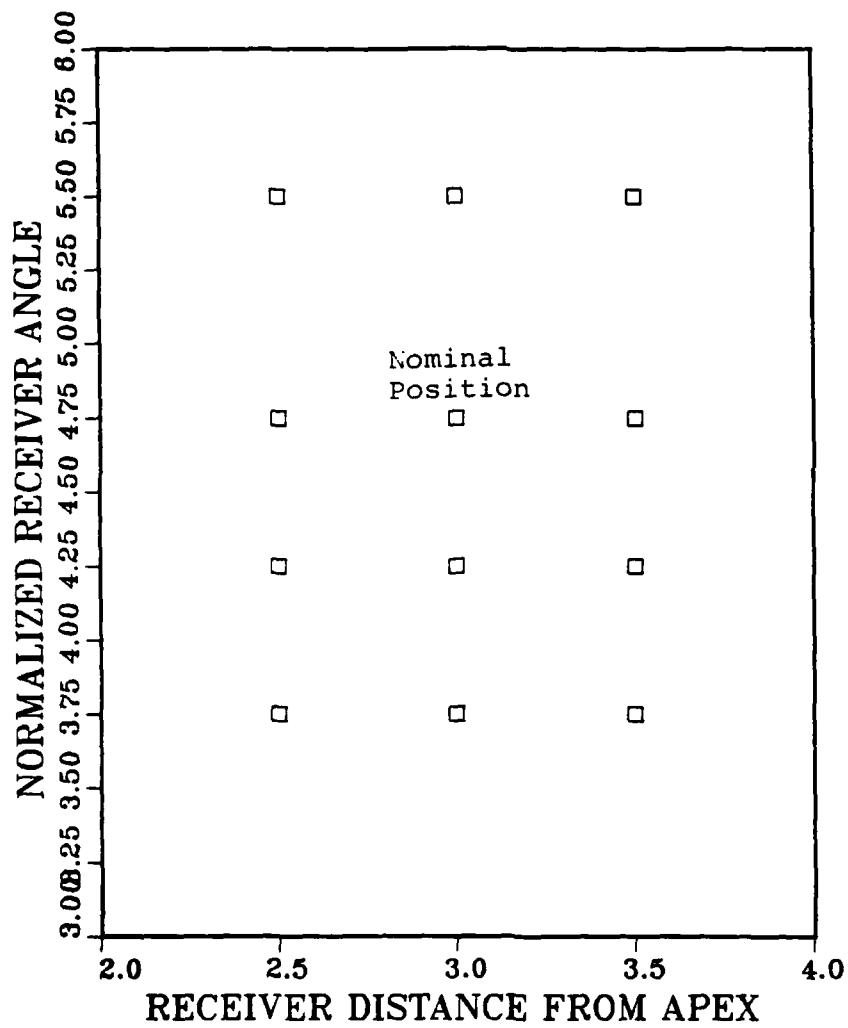


Figure 36. Grid for Determining Sound Pressure in the Wedge

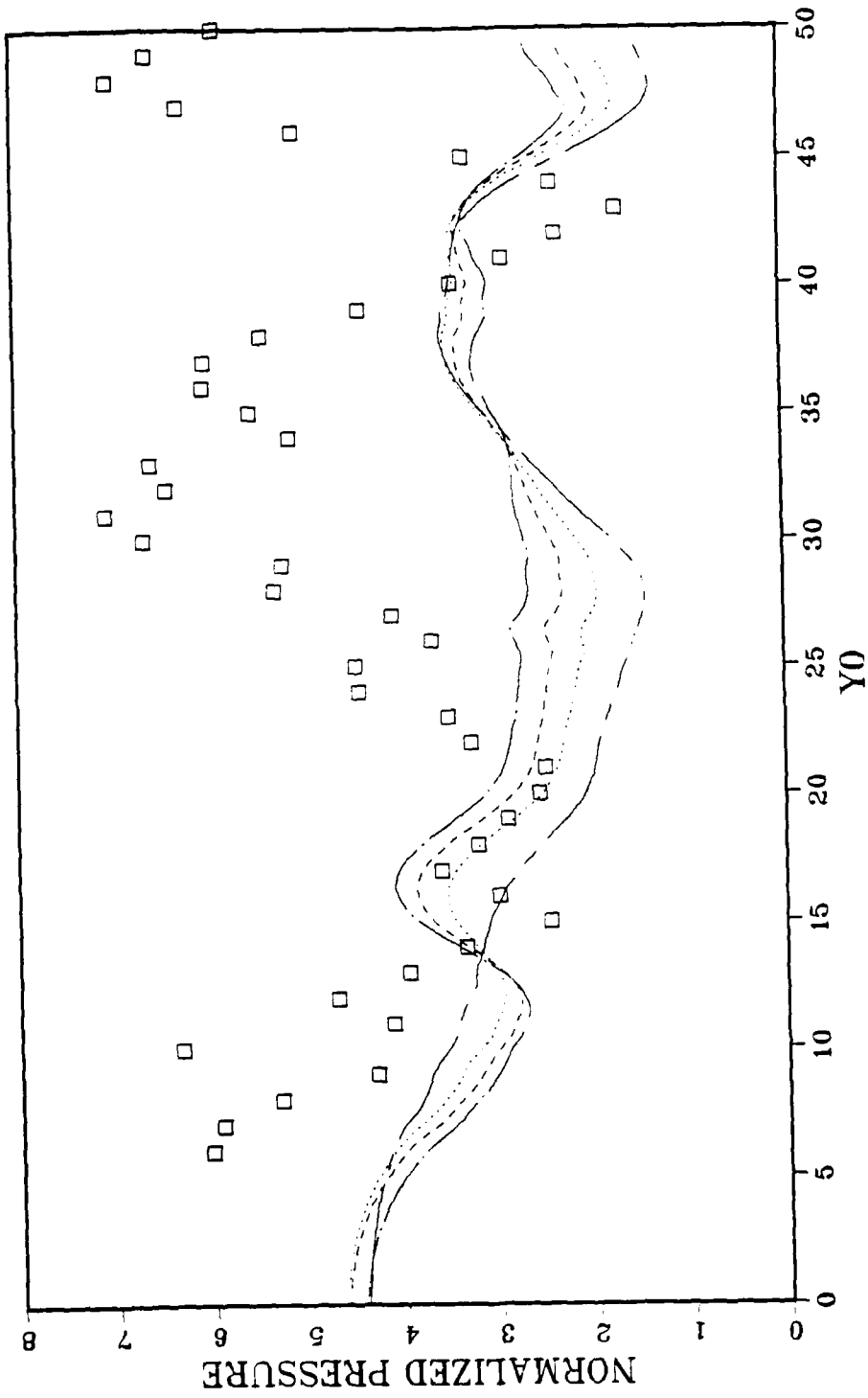


Figure 37. Sound Pressure in the Wedge, $R_2 = 2.5$, $D = 4.75$
 (□ experimental, ... $D = 4.25$ predicted, --- $D = 4.75$
 predicted, -.-. $D = 3.75$ predicted, ---- $D = 5.5$ predicted)

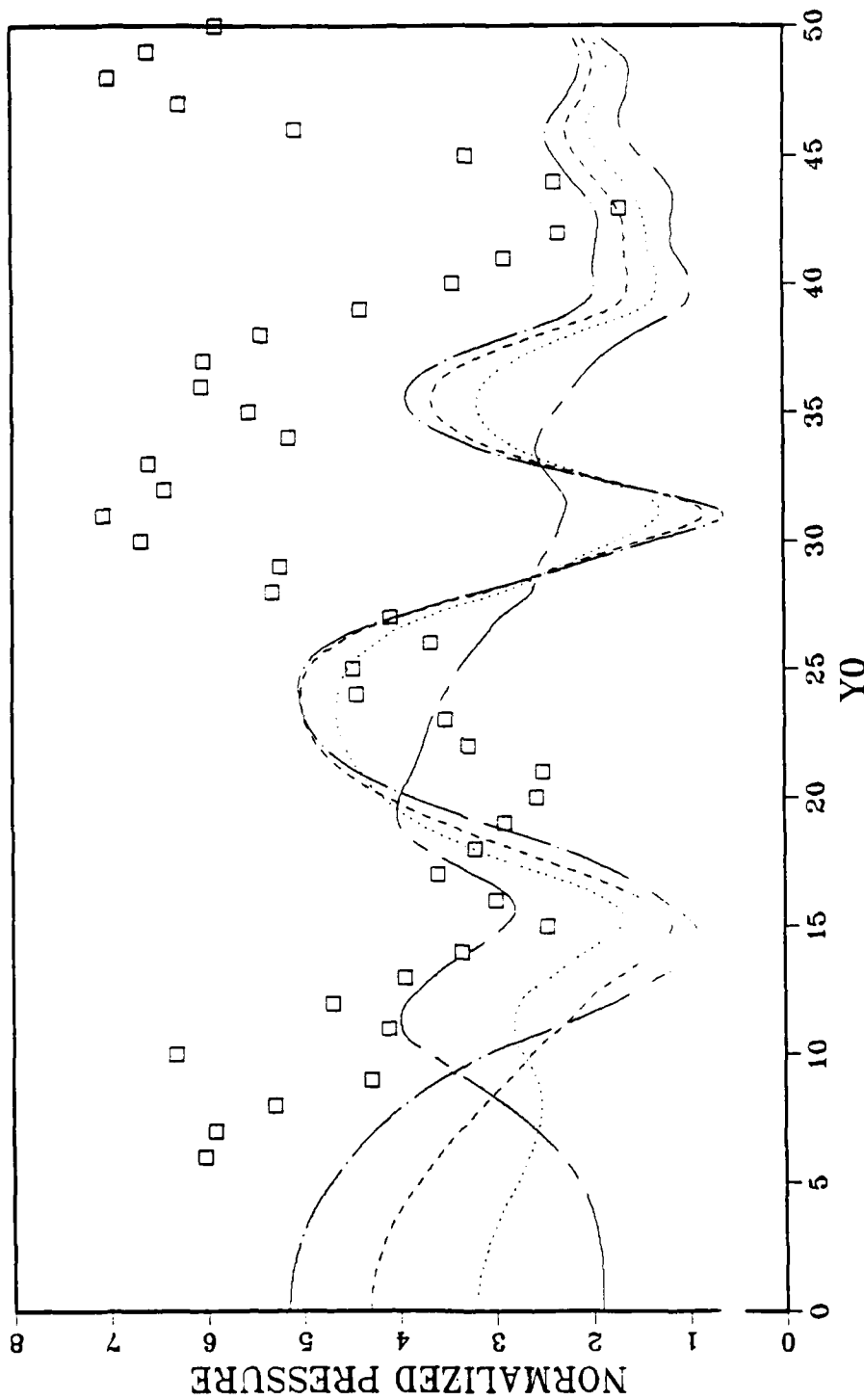
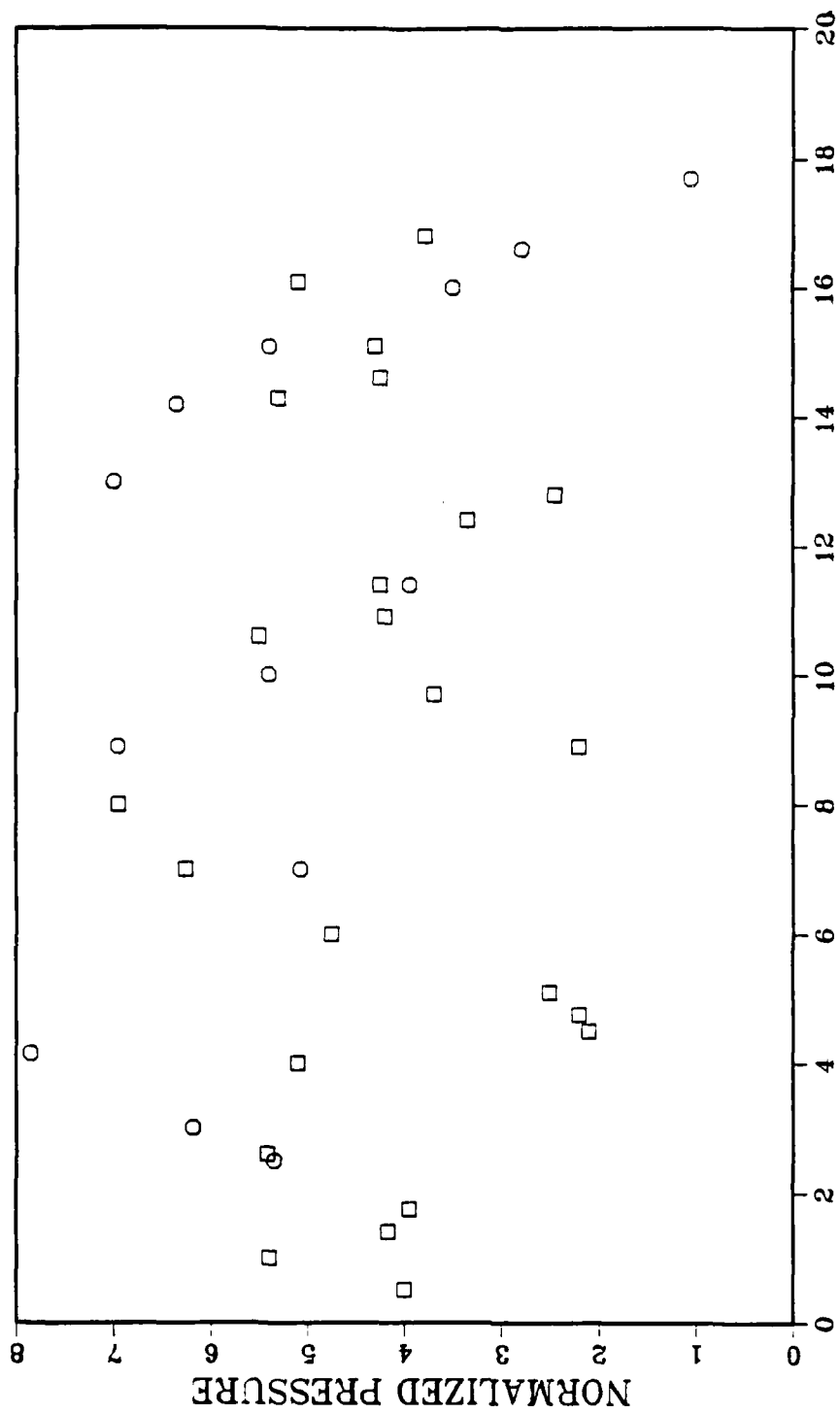


Figure 38. Sound Pressure in the Wedge, $R_2 = 3.5$, $D = 4.75$
 (□ experimental, ... $D = 4.75$ predicted, --- $D = 4.25$
 predicted, -.-. $D = 3.75$ predicted, ----- $D = 5.5$ predicted)



RECEIVER DISTANCE FROM THE APEX

Figure 39. Loci of Pressure Maxima in the Wedge, $Y_0 = 8$, $D = 4.75$
(O experimental, □ predicted)

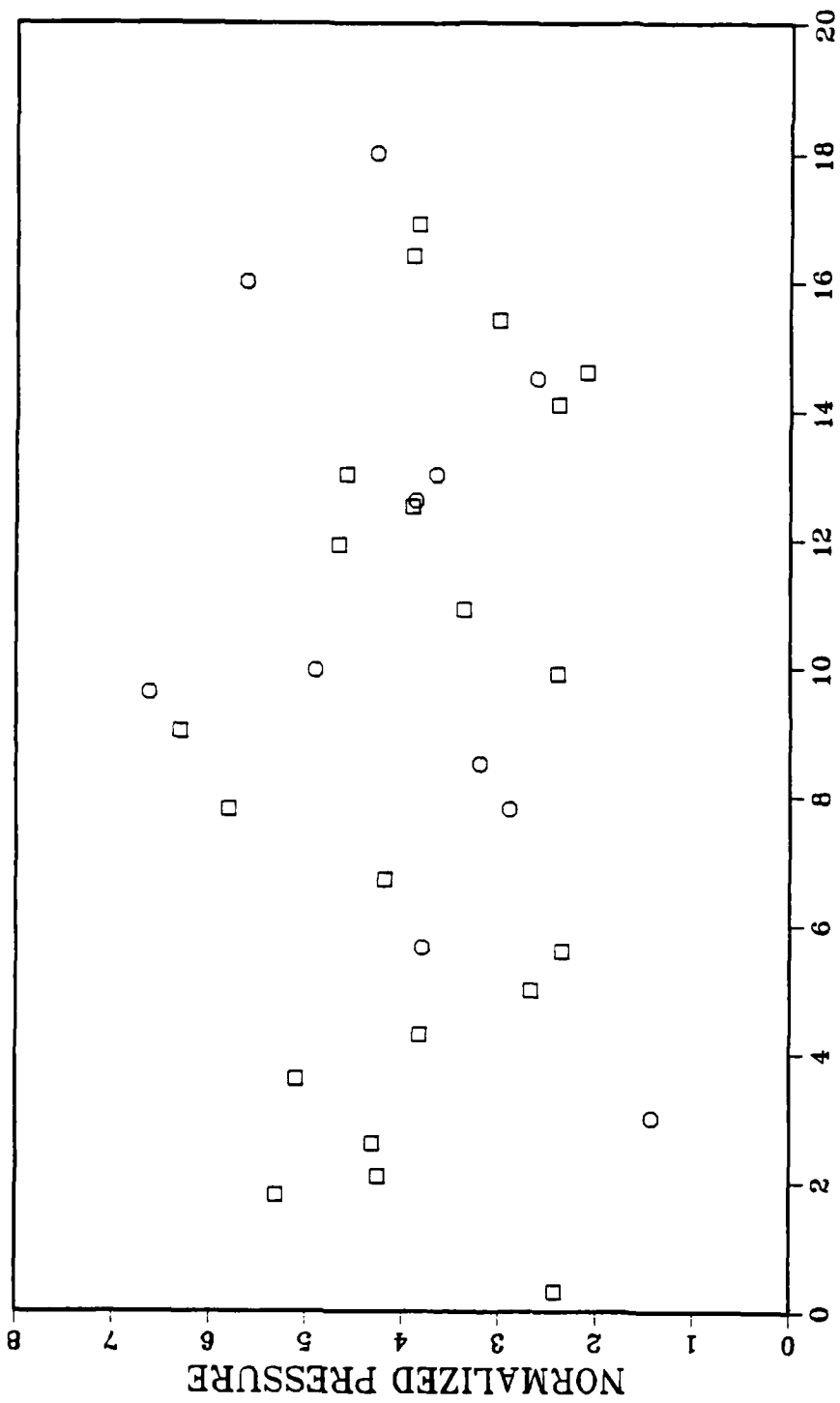


Figure 40. Loci of Pressure Maxima in the Wedge, $Y_0 = 16$, $D = 4.75$
 (O experimental, \square predicted)

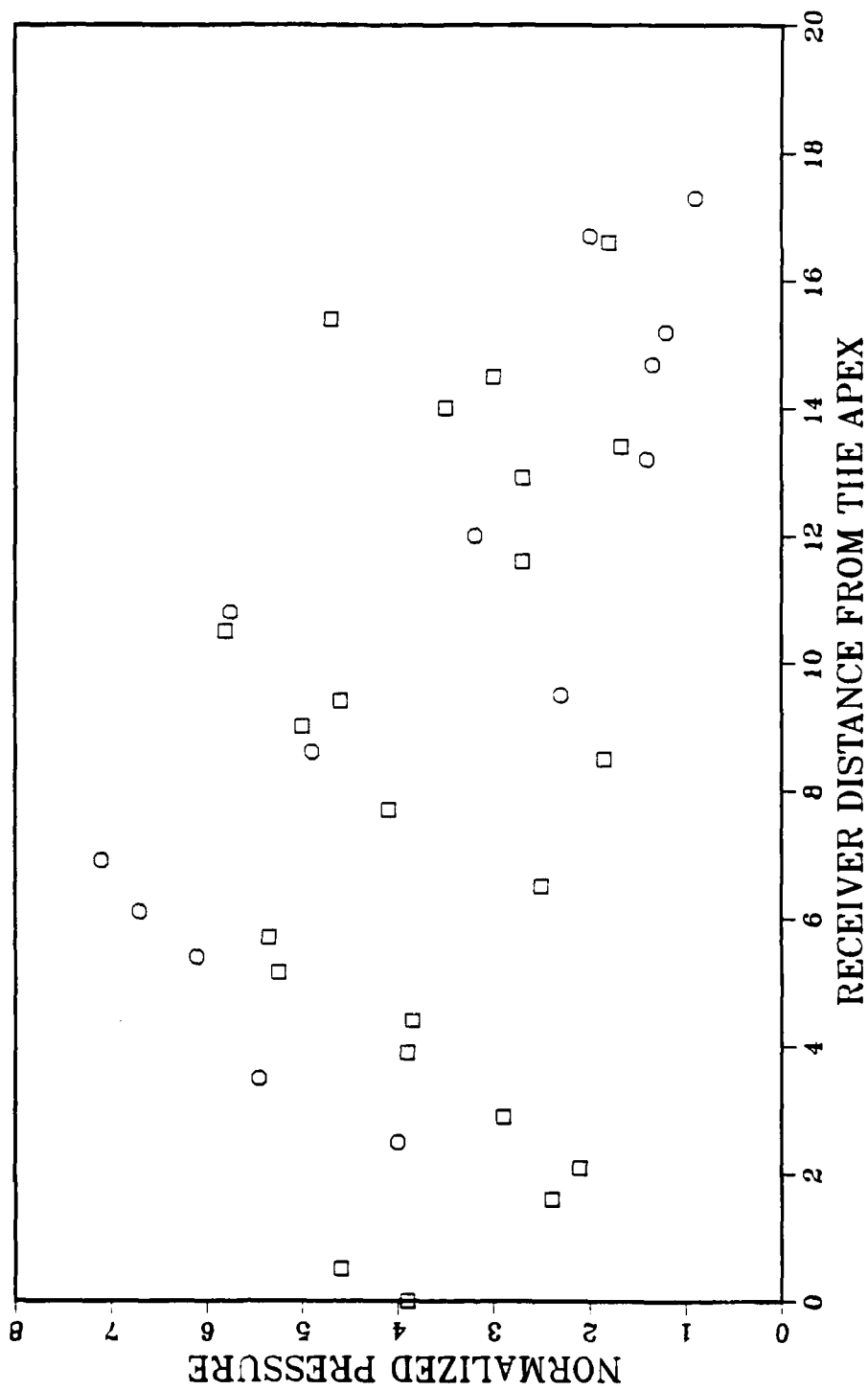


Figure 41. Loci of Pressure Maxima in the Wedge, $Y_0 = 24$, $D = 4.75$
 (O experimental, () predicted)

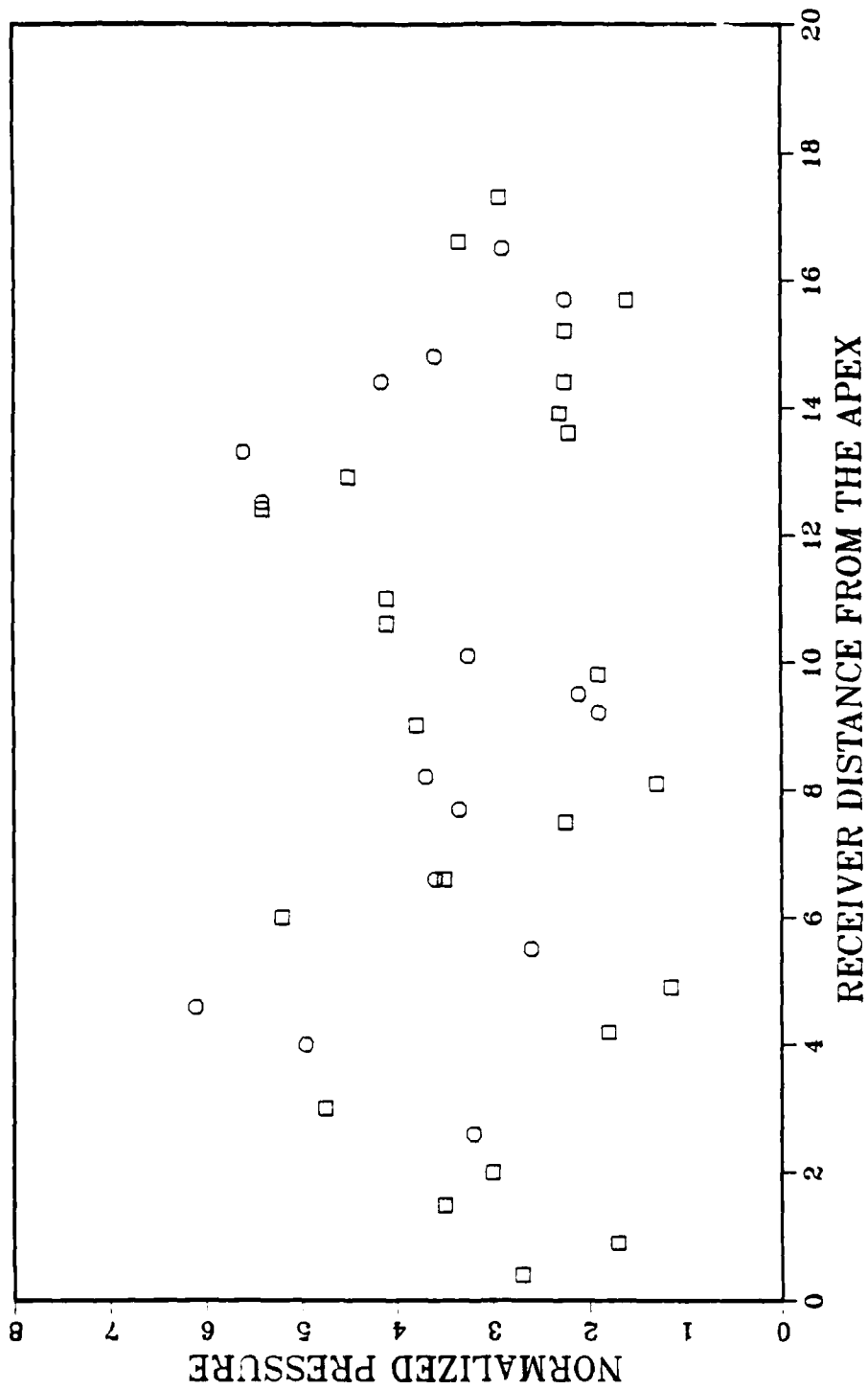


Figure 42. Loci of Pressure Maxima in the Wedge, $Y_0 = 32$, $D = 4.75$
 (O experimental, □ predicted)

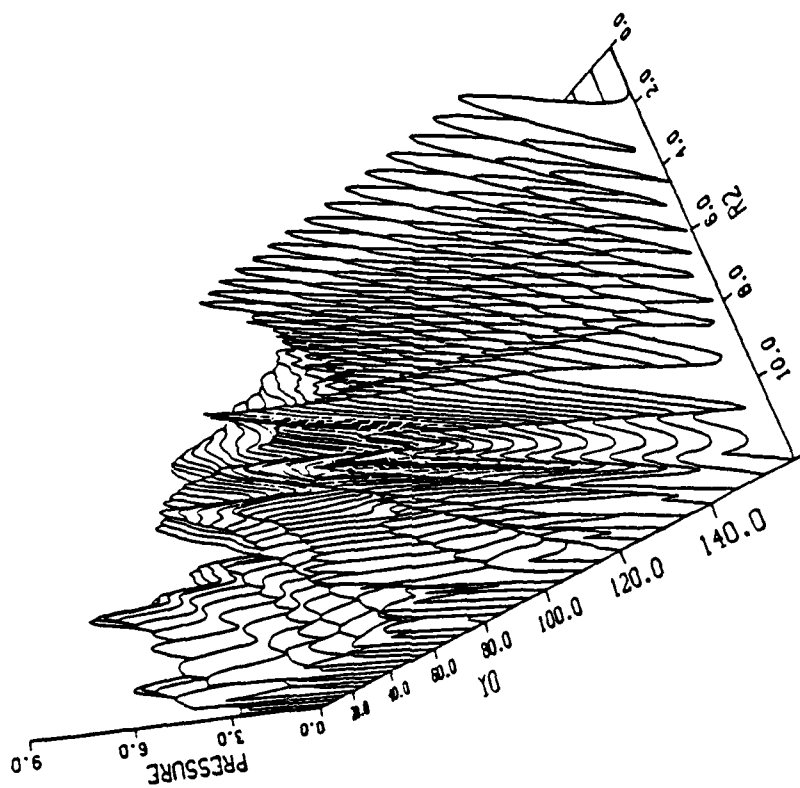


Figure 43. Pressure on Bottom of Wedge as Calculated by Image Model, $B = 10$, $C = 5$, $D = 5.0$, $R_1 = 40$

LIST OF REFERENCES

1. Tien, P.K., and Martin, R.J., "Experiments on Light Waves in a Thin Tapered Film and a New Light-Wave Coupler," Applied Physics Letters, V. 18, p. 398-401, 1 May 1971.
2. Kuznetsov, V.K., "Emergence of Normal Modes Propagating in a Wedge on a Half-Space from the Former into the Latter," Soviet Physical Acoustics, V. 19, p. 241-245, Nov.-Dec. 1973.
3. Naval Postgraduate School Technical Report 5929, Numerical Solutions of Underwater Acoustic Wave Propagation Problems, by Lee, D., and Papadakis, J.S., February 1979.
4. Jaeger, L.E., A Computer Program For Solving The Parabolic Equation Using An Implicit Finite-Difference Solution Method Incorporating Exact Interference Conditions, M.S. Thesis, Naval Postgraduate School, Monterey, California, September 1983.
5. Kosnik, M.E., The Implicit Finite-Difference (I.F.D.) Acoustic Model in a Shallow Water Environment, M.S. Thesis, Naval Postgraduate School, Monterey, California, 1984.
6. Naval Postgraduate School Technical Report 61-79-002, Two Computer Programs for the Evaluation of the Acoustical Pressure Amplitude and Phase at the Bottom of a Wedge-Shaped Fluid Layer Overlaying a Fast Fluid Half Space, by A.B. Coppens, J.V. Sanders, G.I. Ioannou, and W. Kawamura, December 1978.
7. Bradshaw, N.A., Propagation of Sound in a Fast Bottom Underlying a Wedge-Shaped Medium, M.S. Thesis, Naval Postgraduate School, Monterey, California, 1980.
8. Netzorg, G.B., Sound Transmission From a Tapered Fluid Layer into a Fast Bottom, M.S. Thesis, Naval Postgraduate School, Monterey, California, 1977.
9. Bradshaw, J.A., Laboratory Study of Sound Propagation Into a Fast Bottom Medium, M.S. Thesis, Naval Postgraduate School, Monterey, California, June 1981.
10. Coppens, A.B., Humphries, M., and Sanders, J.V., "Propagation of Sound Out of a Fluid Wedge Into an Underlying Fluid Substrate of Greater Sound Speed," Journal Acoustical Society AM.7H(5), November 1984.

11. Baek, C.K., The Acoustic Pressure in a Wedge-Shaped Water Layer Overlaying a Fast Fluid Bottom, M.S. Thesis, Naval Postgraduate School, Monterey, California, 1984.
12. LeSesne, P.K., Development of Computer Programs using the Method of Images to Predict the Sound Field in a Wedge Overlaying a Fast Fluid and Comparison with Laboratory Experiments, M.S. Thesis, Naval Postgraduate School, Monterey, California, December 1984.
13. Coppens, Personal Communication, Naval Postgraduate School, Monterey, California, 1984.
14. Naval Research Laboratory Report 8793, Acoustic Propagation in a Wedge-Shaped Ocean with Perfectly Reflecting Boundaries, by M.J. Buckingham, 1984.

INITIAL DISTRIBUTION LIST

	No. Copies
1. Defense Technical Information Center Cameron Station Alexandria, Virginia 22304-6145	2
2. Library, Code 0142 Naval Postgraduate School Monterey, California 93943-5100	2
3. Dr. J.V. Sanders, Code 61Sd Naval Postgraduate School Monterey, California 93943-5100	5
4. Dr. A.B. Coppens, Code 61Cz Naval Postgraduate School Monterey, California 93943-5100	2
5. Department Library, Code 61 Department of Physics Naval Postgraduate School Monterey, California 93943-5100	1
6. Department Chairman, Code 61 Department of Physics Naval Postgraduate School Monterey, California 93943	1
7. Lcdr J.A. Borchardt 503 N. Palos Verdes Street San Pedro, California 90731	3
8. Lt. Patrick LeSesne 1711 Tipton Drive Crofton, Maryland 21114	1

END

FILMED

4-86

DTIC